A&A 516, A104 (2010)
DOI: 10.1051/0004-6361/200913434

Astronomy & Astrophysics

Massive star formation in Wolf-Rayet galaxies⋆

III. Analysis of the O and WR populations

Á. R. López-Sánchez[1,2] and C. Esteban[2,3]

[1] CSIRO Astronomy & Space Science/Australia Telescope National Facility, PO BOX 76, Epping, NSW 1710, Australia
e-mail: Angel.Lopez-Sanchez@csiro.au
[2] Instituto de Astrofísica de Canarias, C/ Vía Láctea S/N, 38200, La Laguna, Tenerife, Spain
[3] Departamento de Astrofísica de la Universidad de La Laguna, 38071, La Laguna, Tenerife, Spain

Received 9 October 2009 / Accepted 28 March 2010

ABSTRACT

Aims. We perform a comprehensive multiwavelength analysis of a sample of 20 starburst galaxies that show a substantial population of Wolf-Rayet (WR) stars. In this paper, the third of the series, we present the analysis of the O and WR star populations within these galaxies.

Methods. We study the spatial localization of the WR-rich clusters via the detection of the blue WR bump, mainly composed by the broad He II λ4686 line and attributed to WN stars, and the red WR bump, composed by the broad C IV λ5808 line observed in WC stars. We perform a detailed fitting of the nebular and broad emission lines within these broad features and derive the numbers of WN, WC and O stars using (i) the standard assumption of constant WR luminosities and (ii) considering metallicity-dependent WR luminosities. We then compare our results with the predictions given by evolutionary synthesis models and with previous empirical results.

Results. We report the detection of blue WR bump in 20 regions, but the red WR bump is only detected in six. Aperture effects and the exact positioning of the slit onto the WR-rich bursts play a fundamental role in their detection. The nebular He II λ4686 line is detected in 21 regions; its intensity clearly decreases with increasing metallicity. We derive an empirical estimation of the WNL/(WNL+O) ratio using the intensity of the broad He II line assuming metallicity-dependent WR luminosities. As expected, the total number of WR stars increases with increasing metallicity, but objects with $12 + \log(\mathrm{O/H}) < 8.2$ show a rather constant WR/(WR+O) ratio. The computed WCE/WNL ratios are different than those empirically found in nearby star-forming galaxies, indicating that the observed galaxies are experiencing a strong and very short burst. Considering metallicity-dependent WR luminosities, our data agree with a Salpeter-like IMF in all regimes.

Conclusions. We consider that the contribution of the WCE stars is not negligible at low metallicities, but deeper observations are needed to detect the red WR bump because of the decreasing of the WR luminosities with decreasing metallicity. Although available models reproduce the WR properties at high metallicities fairly well, new evolutionary synthesis models for young starbursts including all involved parameters (age, metallicity, star-formation history, IMF and WR stars properties such as metallicity-dependent WR luminosities, stellar rotation and the WR binnary channel) are absolutely needed to perform an appropriate comparison with the observational data.

Key words. galaxies: starburst – galaxies: interactions – galaxies: dwarf – galaxies: abundances – galaxies: ISM – stars: Wolf-Rayet

1. Introduction

Despite their relatively low number and short lifetime in terms of evolutionary timescales, massive stars have a fundamental influence on the interstellar medium (ISM) and galaxy evolution: they generate most of the ultraviolet ionizing radiation in galaxies, powering the far-infrared luminosities through the heating of dust; they enrich the interstellar medium, not only by returning nuclear processed material during their whole lifetime (Maeder 1981) but also in supernova explosions; finally, they deposit mechanical energy, first via strong stellar winds and later as supernovae (Abbott 1982), which are a triggering mechanism of star formation (Woodward 1978). Massive stars are the progenitors of the most energetic phenomena known today, the long gamma-ray bursts (GRB), as they collapse after supernova explotions into black holes (Woosley & Heger 2006). The most massive ($M \geq 25\ M_{\odot}$ for $Z_{\odot}$) luminous (10^5 to $10^6\ L_{\odot}$) and hot (temperatures ~50 000 K) O stars evolve to the Wolf-Rayet phase between 2 and 5 Myr since their birth. A WR star is interpreted as a central He-burning core that has lost the main part of its H-rich envelope via strong winds (Conti 1976; Maeder 1990, 1991). This stage of the most massive stars lasts only some few hundreds of thousands of years ($t_{\mathrm{WR}} \leq 5 \times 10^5$ yr) before they explode as type Ib/Ic supernovae (Meynet & Maeder 2005).

The broad emission features that characterize the spectra of WR stars are often observed in extragalactic H II regions. Actually, these Wolf-Rayet galaxies make up a very inhomogeneous class of star-forming objects, all having in common ongoing or recent star formation which has produced stars massive enough to evolve to the WR stage (Schaerer et al. 1999). The blend of the broad He II λ4686, C III/C IV λ4650 and N III λ4640 emission lines constitutes the blue WR bump; it mainly

⋆ Based on observations made with NOT (Nordic Optical Telescope), INT (Isaac Newton Telescope) and WHT (William Herschel Telescope) operated on the island of La Palma jointly by Denmark, Finland, Iceland, Norway and Sweden (NOT) or the Isaac Newton Group (INT, WHT) in the Spanish Observatorio del Roque de Los Muchachos of the Instituto de Astrofísica de Canarias.

originates in WN stars with a minor contribution of WC stars. The original blue WR bump detection was made in the blue compact dwarf galaxy He 2-10 by Allen, Wright & Goss (1976). Later, Kunth & Sargent (1981) recognized the importance of this WR bump to characterize the mode of star formation in starbursts (burst versus continuous mode) and developed the first method to empirically derive the WR/O ratio. The blend of the C III λ5698 and C IV λ5808 broad emission lines constitutes the red WR bump. C IV λ5808 is the strongest emission line in WC stars, but it is barely seen in WN stars. The first detections of the red WR bump in integrated galaxy spectra were reported by Kunth & Schild (1986) and Dinerstein & Shields (1986), but it seems to be more difficult to detect than the blue WR bump and it is always weaker than the blue WR bump (Guseva et al. 2000; Fernandes et al. 2004). Actually, the red WR bump is rarely observed at low metallicities. However, both WN and WC stars have been detected in the lowest metallicity ($Z \sim 1/50\ Z_{\odot}$) galaxy known, I Zw 18 (Izotov et al. 1997; Legrand et al. 1997; De Mello et al. 1998).

Although the main feature of WR galaxies is a broad He II λ4686 emission line, a considerable fraction of objects also show the nebular (narrow) He II λ4686 line. This emission line is very rarely found in Galactic H II regions (Garnett et al. 1991; Schaerer et al. 1997) but common in planetary nebulae, and has been sometimes observed in giant H II regions where no WR stars have been detected. Sources with sufficient photons of energy >54 eV are needed to produce the nebular He II emission line, so its origin is still puzzling (Garnett et al. 1991; Garnett 2004). Some observations concluded that this nebular line is intimately linked with the appearance of hot WR stars (Schaerer et al. 1996; Schaerer & Vacca 1998; Crowther & Hadfield 2006) but recent analyses suggest that O stars may also contribute to the He II ionizing flux at low metallicities (Brichmann et al. 2008, hereafter BKD08). In one way or in another, studies of the nebular He II emission line give clues about the physical processes in H II regions, the ionizing fluxes of starbursts and their contribution to the ionization of the intergalactic medium (Garnett et al. 1991; Schaerer et al. 1998; Stasińska 1998). This is the reason why Schaerer et al. (1999) also compiled all the extragalactic objects (54) showing the nebular He II λ4686 emission line in their catalog of WR galaxies. The analysis performed by Thuan & Izotov (2005) listed 465 Blue Compact Dwarf galaxies (BCDGs) showing nebular He II λ4686 emission.

Wolf-Rayet stars can be individually observed in our Galaxy, the Magellanic Clouds, in some galaxies of the Local Group (M 31, M 33, IC 10, NGC 6822, IC 1613) and in the brightest galaxies of the Sculptor group (NGC 300 and NGC 55). A recent review of the physical properties of WR stars was presented by Crowther (2007). Thanks to the analysis of these individual WR stars a quantitative classification in WN, WC and WO stars could be established. This led the developing of stellar population synthesis models tailored to the analysis of massive star populations in young starburst galaxies. The best example of these models are those presented by Schaerer & Vacca (1998, hereafter SV98), which provide detailed predictions of many stellar and nebular UV/optical features. Famous Starburst 99 models (Leitherer et al. 1999; Vázquez & Leitherer 2005) also include predictions for the WR and O stars populations. Except for some very low metallicity objects, a good agreement between the observations and the synthesis models of SV98 is usually found. For objects with subsolar metallicity (mostly BCDGs), this comparison indicates fairly short timescales of star formation, with burst ages lower than 2–4 Myr, which is the initial mass function (IMF) compatible with a Salpeter slope, but requires the existence of high-mass stars (Guseva et al. 2000; De Mello et al. 1998; Mas-Hesse & Kunth 1999; Fernandes et al. 2004; Buckalew et al. 2005). However, some authors (Zhang et al. 2007) suggested a dependence of the slope of the IMF on metallicity. The timescales of star formation in high-metallicity enviroments are more extended than those found at low metallicity, with burst durations of 4–10 Myr (Schaerer et al. 2000; Fernandes et al. 2004), although observations are also explained assuming a superposition of several bursts.

We performed a detailed photometric and spectroscopic analysis of a sample of 20 WR galaxies. Our main aim is the study of the formation of massive stars in starburst galaxies and the role that the interactions with or between dwarf galaxies and/or low surface brightness objects have in its triggering mechanism. In Paper I (López-Sánchez & Esteban 2008) we explained the motivation of this work, compiled the list of the analyzed WR galaxies (Table 1 of Paper I) and presented the results of optical/*NIR* broad-band and Hα photometry. In Paper II (López-Sánchez & Esteban 2009) we presented the results of the analysis of intermediate-resolution long-slit spectroscopy of 16 objects of our sample of WR galaxies – the results for the other four objects were published separately. In many cases, two or more slit positions were used to analyze the most interesting zones, knots or morphological structures belonging to each galaxy or even surrounding objects. In this paper we analyze the localization and the properties of the O and WR populations within those galaxies. Papers IV (López-Sánchez & Esteban 2010) and V (López-Sánchez 2010) will present the global multiwavelength analysis of our WR galaxy sample considering all available data.

In Sect. 2 we describe the detection of the WR features. The procedure used to fit the broad and nebular emission lines in the blue and red WR bumps is explained in Sect. 3. We analyze the detection of the nebular He II λ4686 line in Sect. 4. The quantitative analysis of the WNL and WCE star populations in described in Sect. 5. In Sect. 6 we analyze the metallicity dependence of the WR/(WR+O) ratio. The comparison with Schaerer & Vacca (1998) and Starburst 99 (Leitherer et al. 1999; Vázquez & Leitherer 2005) models is shown in Sect. 7. We analyze the derived WCE/WNL ratio in Sect. 8, while the dependence of the IMF on the WR/(WR+O) ratio is discussed in Sect. 9. Finally, we compile our main conclusions in Sect. 10.

2. Detection of the WR features

As our galaxy sample was extracted from the catalog of Wolf-Rayet galaxies compiled by Schaerer et al. (1999), we first analyze the presence or absence of the WR features in the star-forming bursts within our starburst galaxies and the characteristics of their WR populations. Table 1 compiles the objects or regions where any WR bump and/or the nebular He II λ4686 emission line have been detected. Figures 36 and 37 in Paper II show the details of the optical spectrum in the 4600–4750 Å and the 5550–6000 Å ranges, respectively, of all important objects (faint regions with very low S/N have been excluded).

The nebular He II λ4686 emission line is detected in 21 regions within 16 systems (Fig. 36 in Paper II). It is unambiguously clear in 14 objects (HCG 31 AC and F1, Haro 15 A, Mkn 5, POX 4, UM 420, SBS 0926+606 A, SBS 0948+532, SBS 1415+437 C, Tol 1457-262 A and B, ESO 566-8 and NGC 5253 A and D), and particularly strong in POX 4.

The blue WR bump is clearly detected in many objects (Fig. 36 in Paper II), and unambiguously observed in 12

Table 1. Detection of WR features and the nebular He II emission line for the galaxies analyzed in this work.

Galaxy	Zone	Hβ		η	He II λ4686		Blue WR bump[c]		Red WR bump[d]	
		I (a)	$-W$ [Å]		$I/I(H\beta)$ (b)	$-W$ [Å]	$I/I(H\beta)$ (b)	$-W$ [Å]	$I/I(H\beta)$ (b)	$-W$ [Å]
HCG 31	AC[e]	46.13 ± 0.18	91.1 ± 2.1	0.25	0.9 ± 0.3	0.66 ± 0.22	3.2 ± 1.9	2.5 ± 0.6	2.4 ± 0.6	3.1 ± 0.8
	F1	3.187 ± 0.016	218 ± 13	0.80	2.8 ± 0.3	4.3 ± 0.4	...	...	...	...
	F2	2.28 ± 0.19	256 ± 43	0.80	2.2 ± 0.5	3.9 ± 1.5	0.95 ± 0.35	3.4 ± 1.6	...	...
Mkn 1087	C[f]	78.1	...	0.25	...	...	10.6	...	...	...
Haro 15	C	23.3 ± 1.1	16.4 ± 1.1	0.40	0.49:	0.08:	2.82:	0.5:	...	...
	A	23.4 ± 0.9	75.7 ± 4.2	0.50	1.7 ± 0.4	1.0 ± 0.2	1.4 ± 0.5	1.0 ± 0.3	...	...
Mkn 1199	C[e]	74.2 ± 3.1	21.4 ± 1.3	0.50	0.24:	0.05:	6.3 ± 1.8	1.3 ± 0.3	9.4 ± 2.3	2.8 ± 0.7
Mkn 5	A	17.7 ± 0.7	75 ± 5	0.40	0.9 ± 0.2	1.6 ± 0.3	1.5 ± 0.5	3.0 ± 1.2	...	...
IRAS 08208+2816	C	12.9 ± 0.5	80 ± 5	0.25	...	...	4.1 ± 1.3	3.3 ± 1.0	3.5 ± 1.3	3.6 ± 1.4
IRAS 08339+6517	#1	36.5 ± 1.3	25 ± 2	0.50	0.48:	0.1:	4.1:	2.2:	...	...
POX 4	C	56.0 ± 1.8	200 ± 9	0.60	1.20 ± 0.16	1.9 ± 0.3	1.5 ± 0.3	3.0 ± 0.9	1.4 ± 0.2	3.9 ± 0.8
UM 420	...	6.88 ± 0.27	169 ± 10	0.50	1.0 ± 0.2	2.0 ± 0.4	1.5 ± 0.5	2.8 ± 0.7	...	...
SBS 0926+606	A	16.2 ± 0.6	125 ± 6	0.60	0.7 ± 0.2	1.9 ± 0.3	0.9:	3.2:	...	...
SBS 0948+532	...	8.44 ± 0.32	213 ± 11	0.60	1.3 ± 0.3	1.6 ± 0.6	1.1 ± 0.3	2.1 ± 0.7	...	...
SBS 1054+365	C	14.6 ± 0.7	89 ± 7	0.40	0.6 ± 0.2	0.9 ± 0.3	1.6 ± 0.5	2.4 ± 0.8	...	...
SBS 1211+540	...	1.84 ± 0.09	135 ± 10	0.50	...	...	<1.2:	...	NO OBS.[g]	NO OBS.[g]
SBS 1319+579	A	14.6 ± 0.5	285 ± 14	0.90	0.8:	1.5:	0.7:	1.9:	...	...
SBS 1415+437	C	18.5 ± 0.7	222 ± 11	0.60	2.4 ± 0.2	4.8 ± 0.3	<0.9:	...	...	...
III Zw 107	A	22.3 ± 0.8	44.2 ± 2.3	0.50	...	...	3.1 ± 1.1	1.3 ± 0.4	...	...
Tol 9	C	23.4 ± 0.9	33.3 ± 2.0	0.50	0.33 ± 0.15	0.24 ± 0.7	7.9 ± 1.3	2.5 ± 0.4	5.8:	1.9:
Tol 1457-262	A	222 ± 8	101 ± 6	0.50	1.9 ± 0.4	1.5 ± 0.3	...	...	...	...
	B	47.7 ± 2.3	83 ± 7	0.40	2.9 ± 0.3	2.1 ± 0.2	...	...	...	...
ESO 566-7	...	10.2 ± 0.8	13 ± 2	0.25	...	...	...	...	...	...
ESO 566-8	...	111 ± 5	95 ± 7	0.50	0.74 ± 0.25	0.65 ± 0.25	6.2 ± 2.2	4.1 ± 1.5	4.8 ± 1.2	4.2 ± 1.2
NGC 5253	A	134.5 ± 0.4	234 ± 5	1.00	0.10 ± 0.04	0.21 ± 0.09	0.71 ± 0.12	1.6 ± 0.3	NO OBS.[g]	NO OBS.[g]
	B	135.2 ± 4.2	254 ± 5	1.10	0.05:	0.11:	0.71 ± 0.13	1.7 ± 0.3	NO OBS.[g]	NO OBS.[g]
	C[e,g]	101.3 ± 3.3	94.0 ± 1.0	0.40	0.06:	0.05:	4.13 ± 0.19	3.55 ± 0.17	1.00 ± 0.14[h]	NO OBS.[g]
	D	25.6 ± 0.9	39.0 ± 0.5	0.30	0.40 ± 0.11	0.12 ± 0.04	...	...	NO OBS.[g]	NO OBS.[g]

Notes. [(a)] In units of 10^{-15} erg s^{-1} cm^{-2} and not corrected for extinction. [(b)] Assuming $I(H\beta) = 100$ and reddening-corrected. [(c)] Broad He II λ4686 emission line only. [(d)] Broad C IV λ5808 emission line only. [(e)] Broad N III λ4640 also detected. The reddened-corrected $I/I(H\beta)$ ratios are 0.91, 5.6 and 1.44 for HCG 31 AC, Mkn 1199 and NGC 5253 C, respectively. See text for details. [(f)] Data from Vaceli et al. (1997), see López-Sánchez et al. (2004b). [(g)] NO OBS indicates that the spectral range where the feature lies was not observed. [(h)] Broad C IV λ4658 detected. The $I/I(H\beta)$ ratio given here is assuming $L_{WCE}(\lambda5808) = L_{WCE}(\lambda4658)/1.71$ (SV98). See text for details.

regions (HCG 31 AC, Mkn 1199, Mkn 5, IRAS 08208+2816, POX 4, SBS 0948+532, SBS 1054+365, III Zw 107, Tol 9 and NGC 5253 A, B and C). We indicate the spatial localization of the WR stars in each galaxy in Col. 2 of Table 1, sometimes they are detected in different regions within the same system. Our observations of the galaxy IRAS 08339+6517, no cataloged so far as WR, suggest the detection of this kind of massive stars in its central burst (López-Sánchez et al. 2006). Only in three objects previously listed as WR galaxies (Mkn 1087, SBS 1211+540 and ESO 566-7) do we not detect any feature that can be attributed to this kind of massive stars. We consider that aperture effects and the exact positioning of the slit onto the WR-rich bursts play a fundamental role in the detection of the WR features. Furthermore, a good S/N ratio is needed to observe this feature in faint regions. A good spectral resolution is also needed to get a proper deblending of the nebular and broad He II λ4686 lines.

The dominant contribution to the blue WR bump is the broad He II λ4686 line, arising in late type WN stars (WNL). Three regions (HCG 31 AC, Mkn 1199 C and knot C in NGC 5253) show a clear detection of the broad N III λ4640 line, also mainly originated in WNL stars. The absence of the faint N V λ4604 indicates the predominance of WNL stars, although some contribution of early-type WN stars (WNE) might be still present in the blue WR bump (SV98).

As was explained in the introduction, the He II λ4686 emission line and the blue WR bump are mainly linked to WN stars, while the C IV λ5808 emission line (the red WR bump) essentially originates in WC stars. As previous studies indicate, the red WR bump is much more difficult to observe than the blue WR bump. Figure 37 in Paper II shows the spectral range where the red WR bump is located for all important objects; only two galaxies (SBS 1211+540 and NGC 5253) are lacking data in this spectral range. There is always a clear detection of the He I λ5876 line in all spectra, and the faint auroral [N II] λ5755 emission line in also seen in many cases. We clearly identify the broad C IV λ5808 line in 2 galaxies (HCG 31 AC and POX 4), detect it in two galaxies (Mkn 1199 and ESO 566-8) and it also seems to be observed in other two galaxies (IRAS 08208+2816 and Tol 9). However, we do not see this feature in galaxies for which Guseva et al. (2000) reported its detection (HGC 31 G, Mkn 5, UM 420, SBS 0926+606, SBS 0948+532, SBS 1054+365 and SBS 1319+579A). The non-detection of the red WR bump in these objects may be a consequence of aperture effects or the position of the slit, i.e., Guseva et al. (2000) observed slightly different regions than the areas we analyze here. However, our spectra usually have higher spatial and spectral resolution (see Paper II), and even higher signal-to-noise ratio (the average SNR value achieved in this part of the spectra for our galaxy sample is 10–12), particularly those

Fig. 1. Examples of fits to the blue WR bump for some of the analyzed galaxies in the 4620–4750 Å range. The red dotted line represents the position of the He II λ4686 emission line, the blue dotted lines indicate the position of [Fe III] λ4658 and [Ar IV] $\lambda\lambda$4711, 4740 emission lines. The black dashed line represents the continuum fit. The best fit to the observed spectrum (blue continuous line) is shown with a black continuous line, and it is usually composed by the superposition of a broad and a narrow He II λ4686 lines. Region D in NGC 5253 only shows a narrow nebular He II component. The broad N III λ4640 emission feature is detected and fitted in HCG 31 AC and NGC 5253 C. This last region also shows a broad C IV λ4658 emission line, which was included in the fit. The NGC 5253 C also shows the three dashed broad Gaussians that composed the blue WR bump. All diagrams include the residual spectrum after subtracting the best-fit model to the observed spectrum.

obtained using the ISIS spectrograph at the 4.2 m WHT, than the spectra compiled by Guseva et al. (2000), which were obtained using 2 m and 4 m class telescopes (see their Fig. 2). In the past, the non-detection of the red WR bump may have been a detection-threshold effect (the slope in starbursts rises towards the blue and hence on average there are half as many counts in the red WR bump than in the blue WR bump), but we consider this not to be the situation here because of both the quality of our spectra and their relatively good SNR.

The non-detection of the red WR bump could be explained because WC stars are very rarely formed in low-metallicity environments, as evolutionary synthesis models predict and observations suggest (Crowther 2007), indeed our galaxy sample is mainly composed by low-metallicity objects. However, in some objects the non-detection of the red WR bump may be a consequence of a too low S/N ratio. In particular, they should definitively be observed in NGC 5253 given the quality and depth of our spectra. Indeed, the very broad blue WR bump in region C of NGC 5253 strongly suggests the broad C IV λ4658 emission line, with the nebular [Fe III] λ4658 line on top of it (see Fig. 1). We will use this line to estimate the number of WCE stars in this particular zone of NGC 5253.

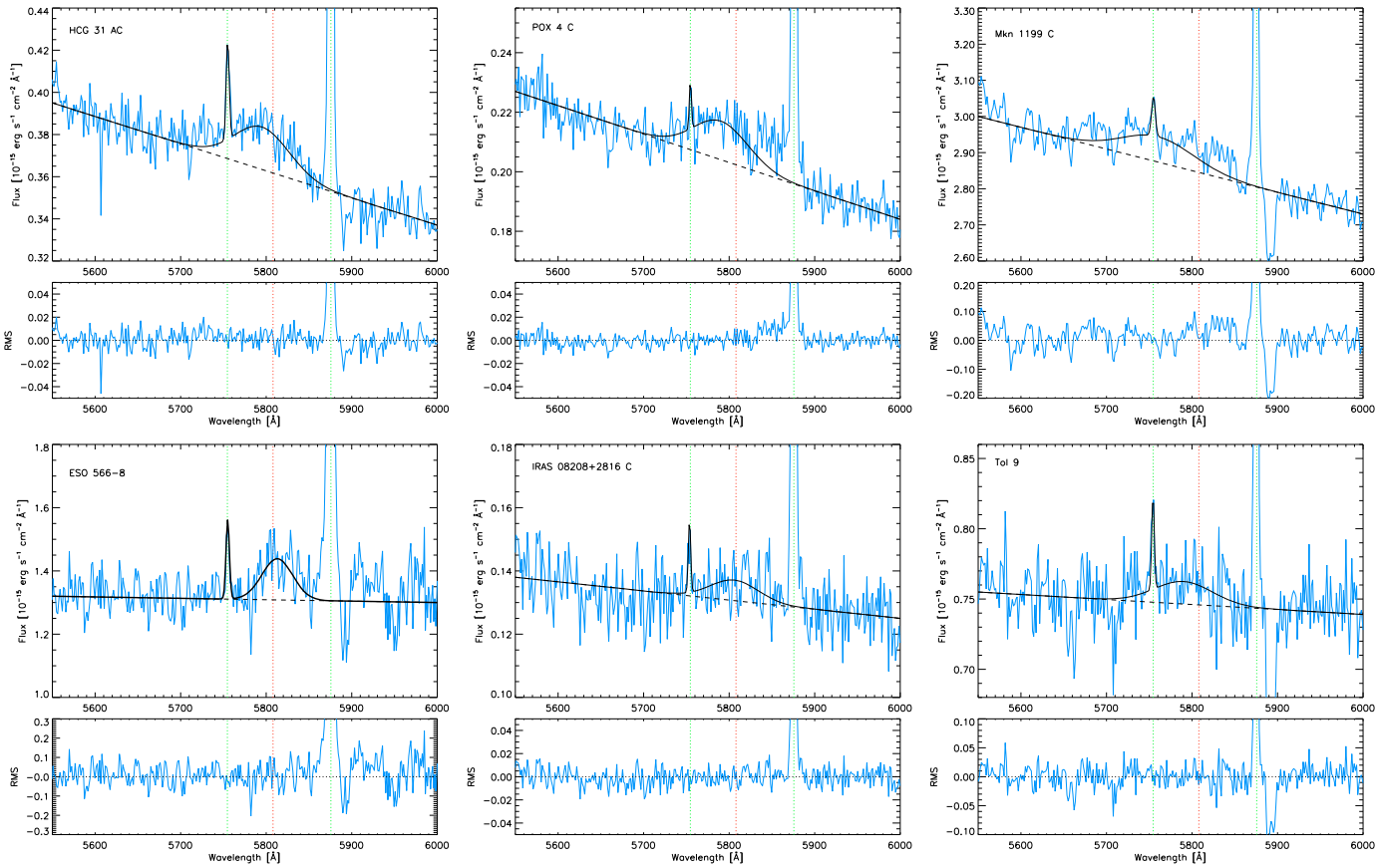

Fig. 2. Examples of fits to the red WR bump for all regions for which we have a detection of the broad C IV λ5808 line in the 5550–6000 Å range. The red dotted line represents the position of the C IV λ5808 emission line, the blue dotted lines indicate the position of [N II] λ5755 and He I λ5875 emission lines. The black dashed line represents the continuum fit. The best fit to the observed spectrum (blue continuous line) is shown with a black continuous line, and it is composed by a broad C IV λ5808 and a nebular [N II] λ5755 line. The broad feature is very evident in HCG 31 AC and in POX 4, detected in Mkn 1199 and ESO 566-8, and probably observed (but with a very low S/N ratio) in IRAS 08208+2816 and Tol 9. Except in POX 4 and IRAS 08208+2816, the spectra also show a clear He I λ5875 absorption feature. All diagrams include the residual spectrum after subtracting the best-fit model to the observed spectrum.

The line C III λ5696, much fainter than the C IV λ5808 line, is not detected in any case. Hence the emission is likely due to early-type WC stars (WCE).

3. Fitting of the WR features

As BKD08 pointed out, the fitting of the WR features, specially in the blue bump, should be done carefully and not only considering one single Gaussian fit. Furthermore, the nebular emission lines within the bump should be properly removed and not included in the flux of the broad stellar lines. Following the procedure described in BKD08, we performed a detailed analysis of each spectrum, checking even those spectra without a clear WR detection. We fitted a broad and a narrow Gaussian for the stellar and nebular He II λ4686 lines in the blue bump and a narrow Gaussian for the nebular [N II] λ5755 emission line ontop a broad Gaussian for the stellar C IV λ5808 line in the red bump. We considered the typical *FWHM* of the nebular lines to constrain the width of the nebular He II λ4686 line and a maximum of *FWHM* $\sim$ 47 Å (σ = 20 Å) in the blue and *FWHM* $\sim$ 59 Å (σ = 25 Å) in the red for the width of the broad stellar lines. This corresponds to *FWHM* $\sim$ 3000 km s^{-1} ($\sigma \sim$ 1280 km s^{-1}), which is an adequate upper limit to the width of individual WR features (BKD08). For the broad He II λ4686 line, all the fits yield $\sigma \leq$ 10 Å except Tol 9 (σ = 13 Å). The fits to the broad C IV λ5808 line were set to the maximum value for Mkn 1199 and Tol 9.

Some examples of this fitting are shown in Figs. 1 (blue WR bump) and 2 (red WR bump). The blue line traces our spectra, the continuum level is indicated by a dashed black line, and the best fit (usually composed by a broad and a nebular He II λ4686 line in the blue bump) is shown with a black continuous line. These figures also show the residual spectrum after subtracting the best-fit model to our observed spectrum. As can be seen, the residual spectra are consistent with Gaussian noise plus the nebular emission lines. We did not consider any fits to the nebular [Fe III] λ4658 and [Ar IV] $\lambda\lambda$4711,4740 lines in the blue range and the nebular He I λ5875 line in the red range because they are clearly seen in the residual spectrum and, considering our spectral resolution, their contribution (if any) to the flux of the WR bumps should be negligible. We want to remark that this careful fitting of the broad and narrow lines was only performed before by BKD08, who used SDSS data; the majority of our spectra have both a higher spectral resolution and S/N ratio than those presented by these authors (compare their Fig. 2 with our Fig. 1). Although BKD08 have a more extensive galaxy sample, the additional strength of our study is the detailed analysis we performed for each region and galaxy (see Papers I and II), which yields a better determination of their properties (chemical abundances, stellar population, star formation

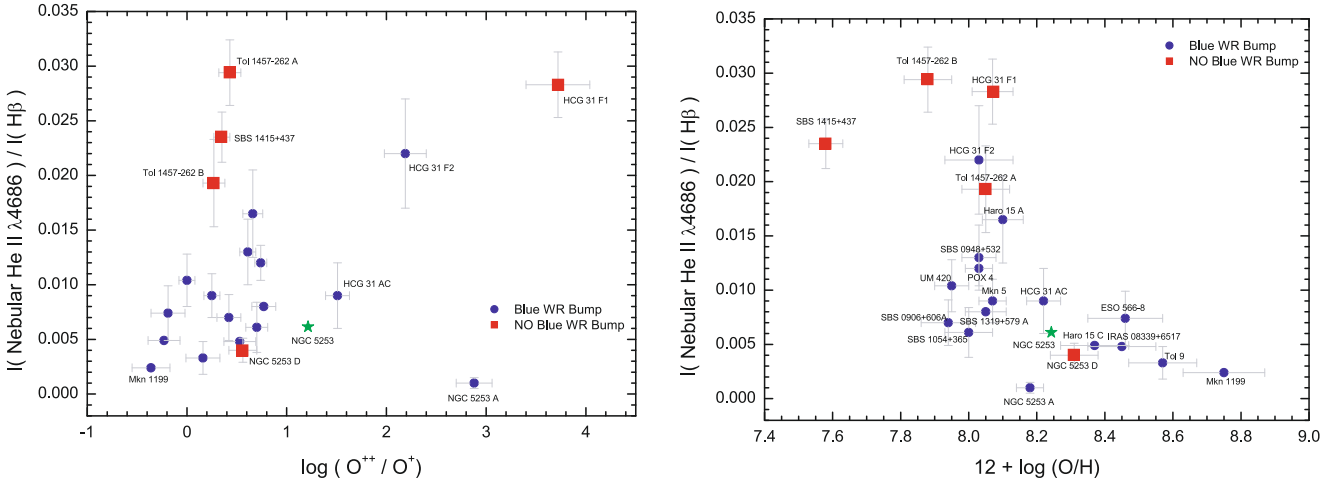

Fig. 3. Intensity of the nebular He II λ4686 line vs. the O^{++}/O^{+} ratio (*left*) and the oxygen abundance (*right*). In both figures, red squares indicate objects in which the nebular He II line but not blue WR bump are detected. Some objects have been labeled. The green star indicates the position of NGC 5253, taking an average value of all analyzed regions.

rate, colors, masses, ...). In particular, we used the bright doublet [O II] $\lambda\lambda$3726, 3729 to estimate the total oxygen abundance, and not the much fainter [O II] $\lambda\lambda$7319, 7330 lines, which usually are the only [O II] lines available in SDSS data. Furthermore, as we will explain in Sect. 7, our galaxy sample is more homogeneous than that used by BKD08, allowing us to perform additional assumptions about their star-formation history.

As seen in Figs. 1 and 2, some spectra reveal very faint WR features. This is the case for region A in SBS 1319+579, for which a very faint blue WR bump and a nebular He II emission line were apparently detected, besides their very low S/N ratio. For the central regions of galaxies IRAS 08208+2818 and Tol 9, the fit of a faint broad C IV λ5808 line also suggests WCE stars. We will consider the values derived from these tentative fits as upper limits to the actual ones.

The broad N III λ4640 line is observed in three objects (HCG 31 AC, Mkn 1199 and NGC 5253 C). We also included this line in the fitting of the data, as Fig. 1 shows. This broad feature is clearly evident in region C of NGC 5253. Incidentally, this region also shows a detection of the broad C IV λ4656 emission line, which was also included in the fit of the blue WR bump.

Table 1 compiles the results of our best fits for the nebular and broad He II λ4686 and the broad C IV λ5808 lines in those regions where these features have been detected. We indicate both the equivalent width and the reddening-corrected $I/I(\mathrm{H}\beta)$ ratios of these lines, including an error estimation for all values. We remind that these features are usually weak, which makes their associated uncertainties considerably high in some cases.

Although we did not observe any WR feature in the two galaxies with the lowest metallicity of our sample (SBS 1211+540 and SBS 1415+437), we estimated an upper limit to the broad He II λ4686 flux. These results are also shown in Table 1.

4. The nebular He II line

As was briefly mentioned in the introduction, there is still some discussion about the origin of the nebular He II λ4686 line. It is generally assumed that the hard radiation field of WR stars produces this nebular line in extragalactic objects (Schaerer 1996, 1998) but some authors are skeptic about this (Garnett et al. 1991; Garnett 2004). The nebular He II λ4686 line may be also produced by hard X-ray radiation from either massive binaries or by supernova remnants from previous generation of stars in the range 10–50 Myr (Pakull & Angebault 1986; van Bever & Vanbeveren 2000; Cerviño et al. 2002) as some observational studies suggest (Bresolin et al. 1999; Guseva et al. 2000; Stasińska & Izotov 2003; Thuan & Izotov 2005), especially at the late stages of the star-formation burst. Garnett (2004) even suggests that as we do not yet understand the evolutionary status of WR stars, it is premature to predict them from stellar evolution models.

Recently, BKD08 re-examined this issue using the SDSS data. They found that the nebular He II λ4686 line was always detected in systems with $\log EW \sim 2.5$ as long as the S/N of the spectrum permitted. In the same way, not *every* galaxy where this nebular line was detected shows WR features, which discrepancy is more pronounced at lower metallicities. As Guseva et al. (2000) already said, in those galaxies (usually very low-metallicity objects) the broad WR feature was very probably too weak to detect. If low-density stellar winds at low-metallicity lead to a higher flux of He II ionizing photons (Smith et al. 2002; Hadfield & Crowther 2007), then normal O stars and not only WR stars would be expect to contribute to the He II ionizing flux. BKD08 finally concluded that although at metallicities higher than 20% solar the ionization of He II is largely produced by WN stars, at lower metallicities it is most likely dominated by O stars, although there should be a probable contribution of WN stars which is undetectable because of the faintness of their optical features.

We compared the intensity of the nebular He II λ4686 emission line with the oxygen abundance and the $\log O^{++}/O^{+}$ ratio. Notice that for NGC 5253 we analyzed four independent regions that are very close one to the other (see López-Sánchez et al. 2007), and hence we also indicate their average values in the diagrams (green stars). In Fig. 3 (*left*) we see that objects with higher excitation tend to show a higher nebular He II λ4686 flux. Regions for which the nebular line is observed but the WR bump is not (HCG 31 F1, SBS 1415+437, Tol 1457-262 A and B and NGC 5253 D) are dispersed throughout the diagram, but all have $\log O^{++}/O^{+} > 0$. On the other hand, the intensity of the nebular He II line clearly decreases with increasing metallicity (Fig. 3, right). Objects in the low-metallicity regime [$12 + \log(\mathrm{O/H}) < 8.2$] have the highest values of the $I(\mathrm{He\,II})/I(\mathrm{H}\beta)$ ratio, and broad

WR features are sometimes not detected in their optical spectra, in agreement with the result found by BKD08. Hence the nebular He II λ4686 emission line *may* arise from ionizing O stars and not only from WN stars at low metallicities. An analysis similar to that shown here involving more galaxies with $12+\log(\mathrm{O/H})<8.2$ and new models of winds of high-mass stars at low metallicities are needed to confirm this assumption. Below we will only consider the broad He II emission line as a clear indication of WR stars within these starburst galaxies.

Guseva et al. (2000) did not find any nebular He II λ4686 line for objects with $12+\log(\mathrm{O/H})>8.13$, concluding that high-metallicity stellar models overpredict the number of photons with $\lambda<228$ Å responsible for the ionization of the He^+. Our careful fitting of the blue WR bump showed that although faint, this nebular line is present in bursts with higher metallicities.

5. Computing of the WR ratios

We estimate the number of WR stars from the luminosity of the broad He II λ4686 line and the broad C IV λ5808 line. Assuming that only WNL stars contribute to the luminosity of the broad He II λ4686 line, we can derive the number of this subtype WR population applying

$$\mathrm{WNL}=N_{\mathrm{WNL}}=\frac{L_{\mathrm{obs}}(\mathrm{He\,II}\,\lambda4686)}{L_{\mathrm{WNL}}(\mathrm{He\,II}\,\lambda4686)}. \quad (1)$$

On the other hand, the number of WCE stars can be computed from the luminosity of the broad C IV λ5808 line:

$$\mathrm{WCE}=N_{\mathrm{WCE}}=\frac{L_{\mathrm{obs}}(\mathrm{C\,IV}\,\lambda5808)}{L_{WCE}(\mathrm{C\,IV}\,\lambda5808)}. \quad (2)$$

For solar metallicities it is well established that one single WNL star contributes with $L_{\mathrm{WNL}}(\mathrm{He\,II}\,\lambda4686)\sim1.7\times10^{36}$ erg s^{-1}, while a single WCE star contributes with $L_{\mathrm{WCE}}(\mathrm{C\,IV}\,\lambda5808)\sim3.3\times10^{36}$ erg s^{-1} (Vacca & Conti 1992). These are the quantity values commonly used (Guseva et al. 2000; Fernandes et al. 2004; Buckalew et al. 2005) and the assumptions considered in the theoretical models (SV98; SB99). However, there is increasing evidence that the WR line luminosities are reduced at lower metallicities (Crowther & Hadfield 2006; Hadfield & Crowther 2006; Crowther 2007). Indeed, Crowther & Hadfield (2006, hereafter CH06) showed how reduced line luminosities at low-metallicity follow naturally if WR winds are metallicity-dependent. Hence we also considered the metallicity of the star-forming regions to get a more appropriate estimation of the number of WR stars. We assumed the broad-line WNL and WCE luminosities given by CH06 for solar and $Z_\odot/50$ metallicites,

$$L_{\mathrm{WNL}}(\mathrm{He\,II}\,\lambda4686,\,Z_\odot)=1.6\times10^{36}\,\mathrm{erg\,s^{-1}}, \quad (3)$$
$$L_{\mathrm{WNL}}(\mathrm{He\,II}\,\lambda4686,\,Z_\odot/50)=2.2\times10^{35}\,\mathrm{erg\,s^{-1}}, \quad (4)$$
$$L_{\mathrm{WCE}}(\mathrm{C\,IV}\,\lambda5808,\,Z_\odot)=2.5\times10^{36}\,\mathrm{erg\,s^{-1}}, \quad (5)$$
$$L_{\mathrm{WCE}}(\mathrm{C\,IV}\,\lambda5808,\,Z_\odot/50)=4.0\times10^{35}\,\mathrm{erg\,s^{-1}}, \quad (6)$$

(see their Tables 3 and 4) and performed a linear fit to these values considering $12+\log(\mathrm{O/H})=8.66$ and 6.96 for $Z_\odot$ (Asplund et al. 2005) and $Z_\odot/50$, respectively. We then adopted for each burst the WR luminosities computed from these relations:

$$L_{\mathrm{WNL}}(\mathrm{He\,II}\,\lambda4686)=(-5.430+0.812x)\times10^{36}\,\mathrm{erg\,s^{-1}}, \quad (7)$$
$$L_{\mathrm{WCE}}(\mathrm{C\,IV}\,\lambda5808)=(-8.198+1.235x)\times10^{36}\,\mathrm{erg\,s^{-1}}, \quad (8)$$

with $x=12+\log(\mathrm{O/H})$. Table 2 compiles the number of WNL stars derived for each burst following both the traditional and the metallicity-depended methods, and the number of WCE stars in objects where the red WR bump was detected following the CH06 assumption. For region C in NGC 5253, we assumed that

$$L_{\mathrm{WCE}}(\mathrm{C\,IV}\,\lambda4658)=1.71\times L_{\mathrm{WCE}}(\mathrm{C\,IV}\,\lambda5808), \quad (9)$$

(SV98) to compute the number of WCE within this knot.

The total number of O stars is derived via the Hβ luminosity, assuming $L_{\mathrm{O7V}}(\mathrm{H}\beta)=4.76\times10^{36}$ erg s^{-1} for a O7V star, $N_{O'}=L(\mathrm{H}\beta)/L(\mathrm{O7V\ H}\beta)$. However, the contribution of the WR stars and other O stars subtypes to the ionizing flux must be considered. This is done via the the $\eta(t)\equiv\mathrm{O7V/O}$ parameter (Vacca & Conti 1992; Vacca 1994; Schaerer & Vacca 1998), which depends on the age of the burst. We used SV98 models (see their Fig. 21) and the estimated age derived for each burst to get an estimation of η (listed in Col. 5 of Table 1), and then applied

$$\mathrm{O}=N_{\mathrm{O}}=\frac{Q_0^{\mathrm{Total}}-N_{\mathrm{WNL}}Q_0^{\mathrm{WNL}}-N_{\mathrm{WCE}}Q_0^{\mathrm{WCE}}}{\eta_0(t)Q_0^{\mathrm{O7V}}}, \quad (10)$$

with Q_0^{Total}, Q_0^{WNL}, Q_0^{WCE} and Q_0^{O7V} the total, the WNL, the WCE and the O7V numbers of ionizing photons, respectively. Following CH06, we assumed $\log Q_0^{\mathrm{WNL}}=49.4$ and $\log Q_0^{\mathrm{WCE}}=49.5$, while we adopted $\log Q_0^{\mathrm{O7V}}=49.0$ (SV98). Q_0^{Total} was derived from $Q_0^{\mathrm{Total}}=N_{O'}Q_0^{\mathrm{O7V}}$. The total number of O stars estimated for each burst are compiled in Table 2. Notice that this table includes several values for the total number of O stars depending on the assumed number of WR stars (only WNL stars following the standard method, only WNL stars considering the metallicity-dependent method, or WNL and WCE stars assuming the metallicity-dependent method). Table 2 also lists the WNL/(WNL+O) ratios derived for the two methods assumed here, and the WCE/(WCE+O), WCE/WNL and WR/(WR+O) ratios computed using the metallicity-dependent method for regions in which WCE stars are detected. The number of WR stars was computed assuming WR = WN + WC = WNL + WCE. For galaxies in which WCE stars are not detected, the total number of WR stars should be the number of WNL stars. However, we must keep in mind that because of the faintness of the broad C IV λ5808 lines (specially at low metallicities), some WCE stars contribution may be also expected, and hence the total number of WR stars assuming WR = WNL is just a lower limit to the actual value.

The last column in Table 2 shows the WR/(WR+O) ratio obtained when applying the empirical relation given by Schaerer & Vacca (1998) between the intensity of the blue WR bump and the WR/(WR+O) ratio,

$$\log\frac{\mathrm{WR}}{\mathrm{WR+O}}=0.85\times\log\frac{I(\mathrm{Blue\ WR\ Bump})}{I(\mathrm{H}\beta)}-0.11. \quad (11)$$

We assumed that the luminosity of the blue WR bump is the luminosity of the broad He II λ4686 line, and added the contribution of the N III λ4640 and the C IV λ4658 to the objects for which these broad lines are detected. As we see, the results provided by this empirical relation are systematically lower than those derived using the direct method (Col. 5 in Table 2) except for the three regions in which other broad emission lines are detected in the blue WR bump. Figure 4 plots the derived WNL/(WNL+O) ratio using CH06 data vs. the intensity of the broad He II λ4686 line. As it can be seen, the best fit to the data shown in Fig. 4 is a quadratic fit,

$$y=-1.511+0.1162x+0.9194x^2, \quad (12)$$

Table 2. O and WR stellar populations for the galaxies analyzed here in which WR features are detected.

Galaxy	Zone	SV98[a]			CH06[b]								
		WNL	O[c]	$\frac{WNL}{WNL+O}$	WNL	O[d]	WCE[e]	O[f]	$\frac{WNL}{WNL+O}$	$\frac{WCE}{WCE+O}$	$\frac{WCE}{WNL}$	$\frac{WR}{WR+O}$	$\frac{WR}{WR+O}$
		[⋆]	[⋆]	(g)	[⋆]	[⋆]	[⋆]	[⋆]	(g,h)	(e)	(e)	(e)	(i)
HCG 31	AC	312	10798	0.028	427	9646	203	7075	0.042	0.028	0.476	0.082	0.051[j]
	F2	4.6	200	0.022	7.1	192	...	192	0.036	...	...	...	0.015
Mkn 1087	C	7181	24680	0.225	7994	16509	...	16509	0.326	...	...	...	0.115
Haro 15	C	347	8806	0.038	432	8271	...	8271	0.050	...	...	...	0.037
	A	173	7963	0.021	257	7542	...	7542	0.033	...	...	...	0.021
Mkn 1199	C	960	6063	0.137	975	5985	932	94	0.140	0.909	0.956	0.953	0.127[j]
Mkn 5	A	2.7	143	0.018	4.1	134	...	134	0.029	...	...	...	0.022
IRAS 08208+2816	C	1344	33338	0.039	1715	29611	932:	17828:	0.055	0.050:	0.543:	0.129:	0.051
IRAS 08339+6517	#1	658	8444	0.072	782	7819	...	7819	0.091	...	...	...	0.050
POX 4	C	122	4346	0.027	191	4058	113	3464	0.045	0.032	0.590	0.081	0.022
UM 420	...	398	17453	0.022	660	16134	...	16134	0.039	...	...	...	0.021
SBS 0926+606	A	32	1987	0.016	54	1897	...	1897	0.028	...	...	...	0.014
SBS 0948+532	...	230	11460	0.020	358	10921	...	10921	0.032	...	...	...	0.017
SBS 1054+365	C	1.1	52	0.020	1.7	48.1	...	1.7	0.034	...	...	...	0.023
SBS 1211+540	...	<0.27	>14.5	<0.018	<0.58	>13	...	>13	<0.043	...	...	...	...
SBS 1319+579	A	6.0	321	0.018	9.2	312	...	312	0.029	...	...	...	0.011
SBS 1415+437	C	<1.0	>62.8	<0.016	<2.4	>57	...	>57	<0.040	...	...	...	...
III Zw 107	A	309	5567	0.053	420	5010	...	5010	0.077	...	...	...	0.041
Tol 9	C	244	981	0.199	272	842	127:	37:	0.244	0.776:	0.469:	0.916:	0.090
ESO 566-8	...	8097	53392	0.132	9574	45975	4768	15839	0.172	0.231	0.498	0.475	0.073
NGC 5253	A	0.73	35.0	0.020	1.03	34.2	...	34.2	0.029	...	...	...	0.012
	B	0.74	32.0	0.022	1.03	31.3	...	31.3	0.032	...	...	...	0.012
	C[k]	3.2	49.2	0.061	4.2	42.8	0.65	37.7	0.090	0.017	0.154	0.114	0.084[j]

Notes. [(a)] We consider the solar value for the luminosity of a single WNL star to the broad He II λ4686 emission line (SV98 method). [(b)] We consider a metallicity-dependent value for the luminosity of a single WNL star to the broad He II λ4686 emission line (CH06 method). [(c)] Total number of O stars after correcting by the ionization of the WNL stars (Eq. (10)) using the SV98 method. [(d)] Total number of O stars after correcting by the ionization of the WNL stars (Eq. (10)) using the CH06 method. [(e)] The number of WCE stars and the WCE/(WCE+O), WCE/WNL and WR/(WR+O) ratios were computed assuming the metallicity-dependent (CH06) method. [(f)] Total number of O stars after correcting by the ionization of the WNL and WCE stars (Eq. (10)) using the CH06 method. [(g)] This coincides with the WR/(WR+O) ratio when no emission from WCE stars is detected. [(h)] This considers the total number of O stars after correcting by the ionization of the WNL and WCE stars derived using the CH06 method. [(i)] Using the empirical calibration given by Schaerer & Vacca (1998, Eq. (11)). [(j)] Considering not only the flux of the broad He II λ4686 flux but also the N III λ4640 and C IV λ4658 fluxes. [(k)] Number of WCE stars computed using the C IV λ4658 line. See text for details.

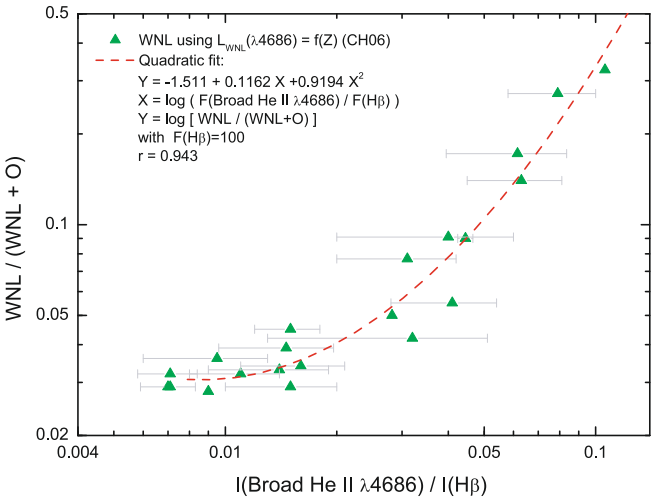

Fig. 4. Number of WNL stars (derived assuming a metallicity-dependence of the WNL luminosities) vs. the reddening-corrected flux of the broad He II λ4686 line. A quadratic fit to the data is shown with a dashed red line.

where $x = \log[I(\mathrm{He\,II}\ \lambda4686)/I(\mathrm{H}\beta)]$ assuming $I(\mathrm{H}\beta) = 100$ and $y = \log[\mathrm{WNL}\ /\ (\mathrm{WNL+O})]$. The correlation coefficient of this fit is $r = 0.943$. A similar relation between the broad C IV λ5808 intensity and the WCE/(WCE+O) ratio seems to be found. However, we did not attempt to fit the data due to the scarcity of observational points.

6. The number of WR stars-metallicity relation

Following evolutionary models of massive stars and population synthesis models (Mas-Hesse & Kunth 1991; SV98; Maeder & Meynet 2005), we should expect an increase of the number of WR stars with increasing metallicity because of the decrease of the minimum mass that a massive star needs to reach the WR phase due to the strong metallicity-dependence of the stellar winds (Vink & de Koter 2005). Kunth & Schild (1986) were the first that noticed that the fraction of WR stars relative to other massive stars increases with increasing metallicity. The analysis performed by Guseva et al. (2000) also showed a tendency between the WR/(WR+O) ratio and the metallicity, and Pindao et al. (2002) reported this dependence for high-metallicity objects. Recent studies indicate that this correlation is certainly satisfied (Zhang et al. 2007; Crowther 2007; BKD08). Besides the uncertainties and considerable high scatter of their data, BKD08 indicated that models of stellar evolution including massive binaries by Eldridge et al. (2008) appear to well reproduce the relation between the metallicity and the number of WR stars even at low metallicity.

Figure 5 plots the evolution of the relative numbers of massive stars, WR/(WR+O), with respect to the oxygen abundance for our galaxy sample. Blue points represent WR = WNL assuming a constant luminosity for the broad He II λ4686,

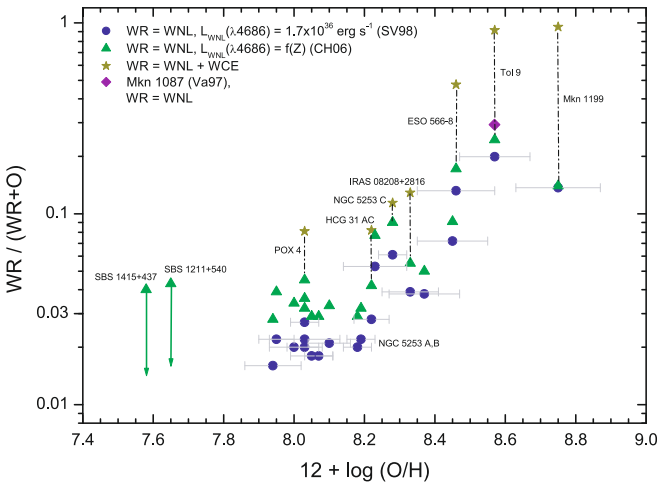

Fig. 5. WR/(WR+O) vs. oxygen abundance for our galaxy sample. Blue points represent WR = WNL assuming a constant luminosity for the broad He II λ4686 emission, green triangles indicate WR = WNL considering a metallicity-dependent broad He II λ4686. Dark yellow stars plot WR = WNL + WCE assuming the metallicity-dependent WNL and WCE luminosities. We include the upper limit to the WR/(WR+O) ratio estimated for the very low-metallicity galaxies SBS 1211+540 and SBS 1415+437. Dashed lines connect the WR = WNL and the WR = WNL + WCE values for the galaxies for which we have WCE data. These galaxies have been labelled.

green triangles indicate WR = WNL considering a metallicity-dependent broad He II λ4686. Dark yellow stars plot WR = WNL + WCE assuming the metallicity-dependent of both WNL and WCE luminosities. From this figure is evident that the number of WR stars increases with increasing metallicity, specially in the high-metallicity regime.

We should expect some scatter in Fig. 5 because of the strong dependence on time of the WR star relative numbers during the short WR stage of the starburst. That is what may be happening in NGC 5253: regions A and B show a low WNL/(WNL+O) ratio, region C has a very intense blue WR bump and a high WNR/(WR+O) ratio, but no broad WR feature is found in region D even though all zones are very close. Actually, as it was explained by Guseva et al. (2000), a galaxy undergoing a star-formation burst would describe a loop in this diagram, quickly reach the WR/(WR+O) maximum and after that drop down to slightly higher metallicities because of the chemical enrichment of the surrounding interstellar medium. We consider that the scatter in Fig. 5 is not so evident because all analyzed objects are undergoing an intense and very probably short star-formation event with an age between 3.5 and 5.5 Myr (see Paper I) and have a very similar nature, with the majority of them BCDGs.

However, Fig. 5 may suggest a possible change of the slope of the relation between the number of WNL stars and the metallicity when considering the metallicity-dependent broad He II λ4686 (green triangles). For galaxies with 12 + log(O/H) > 8.2, the WNL/(WNL+O) ratio clearly increases with metallicity, but in the range 12 + log(O/H) = 7.9–8.2 it seems to become constant, with a value of WNL/(WNL + O) ~ 0.03–0.04 (11 points). We cannot confirm that tendency, however, because of the lack of objects in the range 12 + log(O/H) = 7.6–7.9, and hence more data in the low metallicity regime are needed to understand the metallicity dependence of the WNL/(WNL+O) ratio. This behavior was previously noticed by BKD08 and suggested by Guseva et al. (2000). One of the main problems to acquire these data is that both the WR/(WR+O) ratio and the duration of the WR phase decrease with decreasing metallicity, so the number of galaxies with extremely low metallicity – 12 + log(O/H) $\leq$ 7.8 – containing a WR stellar population is expected to be small. Despite the good spectral resolution and S/N ratio of our WHT spectra, we did not detect a hint of WR stars in any of the regions within our two lowest metallicity galaxies (SBS 1211+540 and SBS 1415+437; their upper limits are plotted in Fig. 5), only the nebular He II λ4686 line in the brightest region of SBS 1415+437. However, WR stars have been detected in the lowest metallicity galaxies known so far: I Zw 18, with $Z \sim Z_{\odot}/50$ (Izotov et al. 1997; Legrand et al. 1997; Brown et al. 2002) and SBS 0335-052E, with $Z \sim Z_{\odot}/40$ (Izotov & Thuan 1999; Izotov et al. 1999; Papaderos et al. 2006).

Ideally, we would also like to compare the WCE and WR = WNL+WCE corrected values between high- and low-metallicity objects, but this is difficult because WCE stars are undetected most of the time, in particular at low metallicities. Considering our data plotted in Fig. 5, the WCE/(WCE+O) ratio also increases with metallicity in galaxies with 12 + log(O/H) $\geq$ 8.2. However, the two lowest metallicity objects in which we detect both WNL and WCE stars, POX 4 and HCG 31 AC, have very similar WNL/(WNL+O), WCE/(WCE+O) and WR/(WR+O) ratios (see Table 2) despite their relatively different oxygen abundance, 12 + log(O/H) = 8.03 and 8.22, respectively. Again, we state that more data of low-metallicity galaxies with clear detections of both the blue and red WR bumps are needed to understand this behavior.

Another interesting information from Fig. 5 is that for all galaxies with a detection of WCE stars the derived WR/(WR+O) ratio is considerably higher than when only WNL stars are considered. The contribution of these WCE stars is smaller at lower metallicities, but even for POX 4 (the lowest metallicity galaxy where both WNL and WCE stars are detected) the WCE stars contribute to the 37% to the total WR number. This as well as the analysis of the WCE/WNL ratio that we will explain below strongly suggests that WCE stars are not only present at low metallicities but also make an important contribution to the total number of WR stars.

7. Comparison with the theoretical models

The first models that tried to quantify the population of WR stars in starbursts were those presented by Arnault et al. (1989), who found that the star-formation event only occurs during a short period of time compared with the typical lifetime of the massive stars and that the intensity of the blue WR bump with respect Hβ decreases with decreasing metallicity. The models presented by Mas-Hesse & Kunth (1991), updated by Cerviño & Mas-Hesse (1994), were the first models that determined the number of WR stars. However, their method had several flaws because they did not separate the stellar emission lines within the blue WR bump, which as we see are also blended with the nearby Fe, He and Ar lines from the emission of the nebular gas. With the aim of solving this problem, Krüger et al. (1992) separately synthesized the broad He II λ4686 and C III/IV λ4650. Meynet (1995) studied the effect of changing the star-formation rate, the IMF, the age and the metallicity in the massive star populations. Although the detailed models provided by Leitherer & Heckman (1995) included a good study of the O and WR populations, they failed to reproduce some observational features. The evolutionary models presented by García-Vargas et al. (1995) had the same problem.

Schaerer & Vacca (1998, hereafter SV98) constructed evolutionary synthesis models for young starbursts using stellar

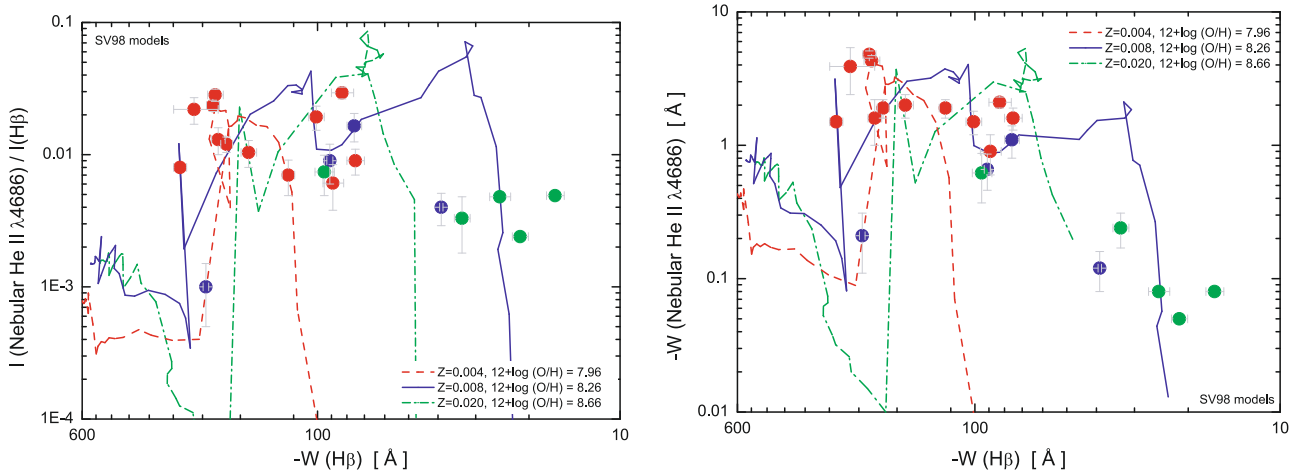

Fig. 6. Intensity (*left*) and equivalent width (*right*) of the nebular He II λ4686 line vs. W(Hβ) and their comparison with the predictions given by SV98 models. Three different metallicities, Z = 0.004, 0.008 and 0.020 ($Z_\odot$) are plotted with dashed red, continuous blue, and dashed-dotted green lines, respectively. Data colors (red, blue and green) indicate the model that best matches the metallicity of the object.

evolution models, theoretical stellar spectra and a compilation of observed line-strengths from WR stars. They explicitly distinguish between several WR stars (WN, WC, WO) whose relative frequency strongly depends on the metallicity, and also consider O and Of stars independently. The SV98 models compute the number of O and WR stars produced during the starbursts and predict the intensities of the UV and optical emission lines of both the main nebular lines (H and He) and the broad stellar lines (He, N and C) as a function of several parameters related to the star-formation episode. These models provide the most reliable determinations to date. The basic framework of the SV98 models was recently included in the STARBURST 99 stellar population synthesis model (Leitherer et al. 1999) with refined spectra from Smith et al. (2002). The last release of the SB99 code (Vázquez & Leitherer 2005) is available on-line[1].

We considered both the SV98 and SB99 models to compare their predictions with our observational data. In both cases we assumed an instantaneous burst with a Salpeter IMF slope α = 2.35 and $M_{\rm up}$ = 120 $M_\odot$ with three different metallicities, Z = 0.004, 0.008 and 0.020 ($Z_\odot$), which correspond to an oxygen abundance – in units of 12 + log(O/H) – of 7.96, 8.26 and 8.66, respectively. The SV98 models consider $M_{\rm low}$ = 0.8 $M_\odot$ and SB99 models assume $M_{\rm low}$ = 0.1 $M_\odot$. Although this does not affect to the predictions for the massive stars, the SB99 models were created assuming Padova tracks in which asymptotic giant branch (AGB) phases with the same metallicity of the gas are included (Vázquez & Leitherer 2005). The total stellar mass created in the starburst (a normalization factor) was set to 1 $M_\odot$ and 10^6 $M_\odot$ for SV98 and SB99 models, respectively.

Besides that the SV98 models are the most reliable WR galaxy models to date, we remind the reader that nowadays there is a better understanding of the properties of the WR stars than when the SV98 models were released. The main refinement is the metallicity-dependence of the He II λ4686 luminosity (CH06) and the influence of the rotation (Meynet & Maeder 2005) and wind loss and binary evolution (van Bever & Vanbeveren 2003; Vanbeveren et al. 2007; Eldridge et al. 2008) in the stellar tracks followed by massive stars. Stellar rotation is expected to predict a longer WR stage, lower WR star masses and thus larger WR populations. BKD08 considered some variations in the WR lines fluxes with the metallicity to update the SV98 models, but these models were not published anywhere. These authors also remarked the importance of the star-formation histories of the galaxies hosting the WR-rich star-clusters, combining their models with the predictions given by both the SB99 and the Bruzual & Charlot (2003) codes to generate a wide range of models that depend on many parameters. New models of evolving starbursts showing WR features that include all these aspects are absolutely needed.

Figures 6–10 compare the predictions of the SV98 and SB99 theoretical models with our observational data. As the luminosity of the WR features and their relative strength compared to other spectral properties depends on age, metallicity, star-formation history, and the IMF, the comparison of the observational data with the models should be carefully done. In all these figures the green dashed-dotted line represents the model predictions for solar metallicities (Z = 0.020), the continuous blue line is the prediction of the Z = 0.008 model and the red dashed line indicates the predictions of the Z = 0.004 models. The color of the observational points is chosen according to the model that better matches their metallicity. We always represent in the x-axis the Hβ equivalent width, W(Hβ), which is a good indicator for the age of the most recent massive star-formation event. Indeed, the hydrogen-ionizing flux of a star cluster gradually decreases as the most massive stars disappear with time, and hence the absolute value of the width of Hβ decreases with time (see Papers I and II). BKD08 questioned the validity of this parameter for a large sample of WR galaxies spanning a wide range in metallicities and sizes, moreover if the spectrum covers a big region in the galaxy including young and old stellar populations. This is not typically our case, because all the spectra analyzed here were mainly obtained in brightest Hα-selected regions within the galaxies (see Paper II) in which the underlying old stellar population is not dominating the optical light. Hence, while the spectroscopic SDSS data used by BKD08 randomly selected a very heterogeneous sample of objects with a fixed fiber size (3″), we first carefully analyzed the position of the brightest H II regions within our sample of WR galaxies (Paper I) and then extracted the spectroscopic data using efficient apertures (Paper II). Furthermore, both the analysis of the Hα imagery and the spectra indicate that all objects have experienced an almost instantaneous star-formation event

[1] http://www.stsci.edu/science/starburst99/

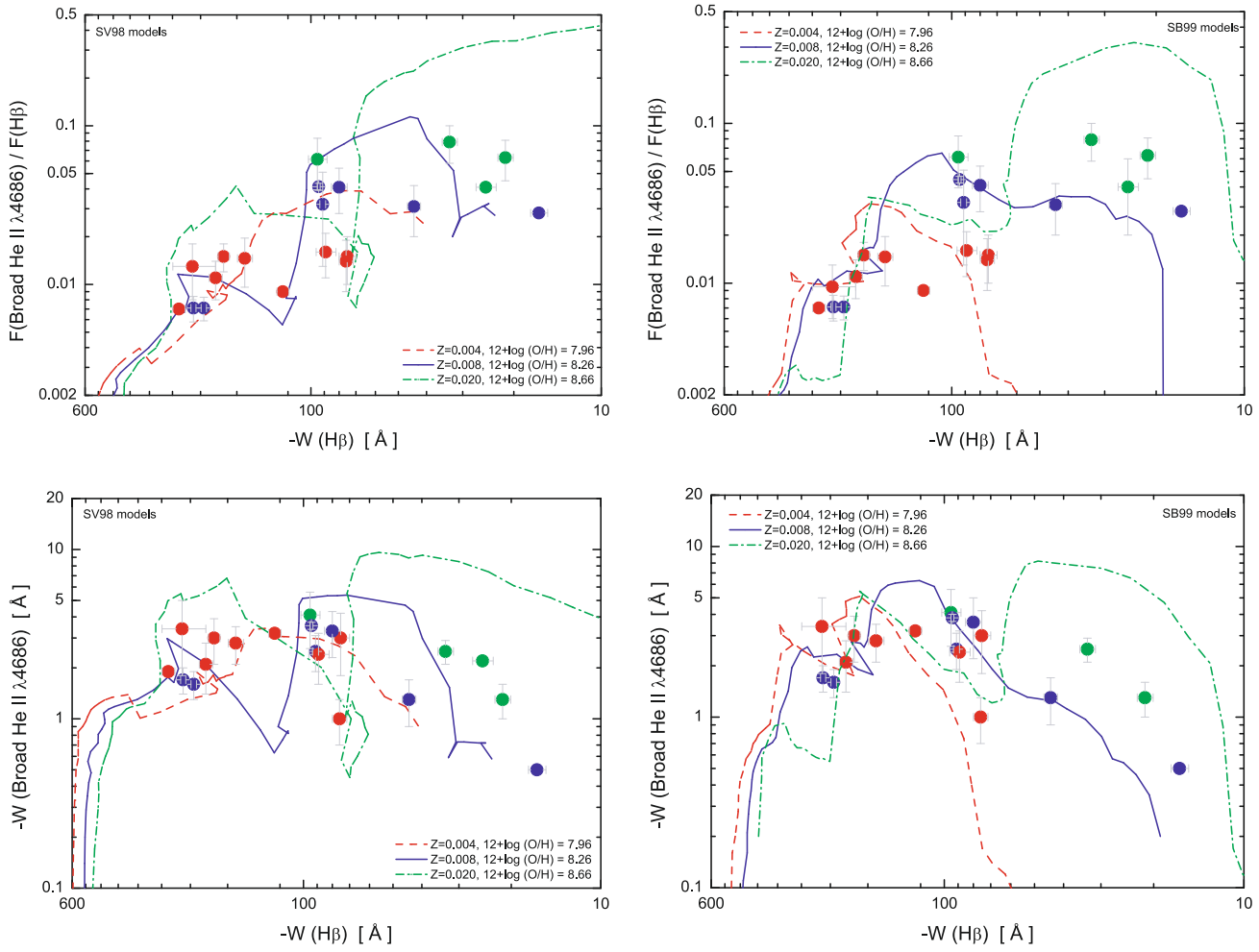

Fig. 7. Comparison of the observed intensities (*upper row*) and equivalent width (*lower row*) of the broad He II λ4686 emission line with the predictions given by SV98 (*left*) and SB99 (*right*) models. Symbols are the same as in Fig. 6.

that happened between 3 and 6 Myr ago. Although some few cases of BCDGs seem to indicate continuous star formation for some few Myr (i.e., Mkn 209, see Pérez-Montero & Díaz 2007), the majority of the analyses of similar low-metallicity galaxies (i.e., Guseva et al. 2000; Cairós et al. 2001, 2007; Gil de Paz & Madore 2005) support the instantaneous star-formation scenario. Hence we consider the comparison of the observational data with a model of a single star-formation event appropriate for our analysis, and that W(Hβ) is a reliable indicator of the age of the starbursts.

Figure 6 compares the predictions of the nebular He II λ4686 following the SV98 models with our data. The diagrams plot the intensity (left panel) and the equivalent width (right panel) of this nebular line as a function of the Hβ equivalent width. Notice that several high-metallicity objects – green dots – with W(Hβ)≥ -60 Å are displaced somewhat to the right of the model predictions in both diagrams. We think that this effect is a consequence of a probable underestimation of the W(Hβ) in these objects, which have more complex star-formation histories and a considerable contribution of the old underlying population than the low- and intermediate-metallicity objects. We should keep this in mind when comparing observed and predicted properties for high-metallicity objects in the next figures. In particular, we should expect a much more complex star-formation history in a spiral galaxy than in a BCDG. In our study, only Mkn 1199, Mkn 1087, ESO 566-8, ESO 566-7, IRAS 08339+6517 and Tol 9, all with 12+log(O/H) > 8.4, show clear complex star-formation histories, although today all of them are hosting a strong starburst. These objects are plotted with green dots in Figs. 6–10. Perhaps their W(Hβ) have been slightly underestimated, but the comparison of their observed emission line properties with the predictions given by the photoionization models provided by Stasińska, Schaerer & Leitherer (2001; see Fig. 10 in Paper IV) indicates that the underestimation of the W(Hβ) value is not very important (10–20 Å at almost). Hence, although the W(Hβ) derived in high-metallicities objects may be somewhat underestimated, we think that it is not the case for low- and intermediate-metallicity objects because (i) the contribution of the underlying stellar population, although it does exist, is not dominating in the strong star-formation bursts (see Sect. 4 in Paper I and its Figs. 37–39) and (ii) the ages of the star-forming bursts obtained from W(Hβ) agree with those determined using independent methods (see Sect. 4 in Paper II and its Fig. 39).

From Fig. 6 (left) is also evident that galaxies with higher metallicities show lower He II λ4686 intensities. As we already discussed, this line is not or only very weakly detected in our highest metallicities objects. Both the He II λ4686 intensity and its equivalent width (Fig. 6, right) decrease with increasing W(Hβ). The model predictions by SV98 generally agree well with our data, but perhaps they overpredict the intensity of the

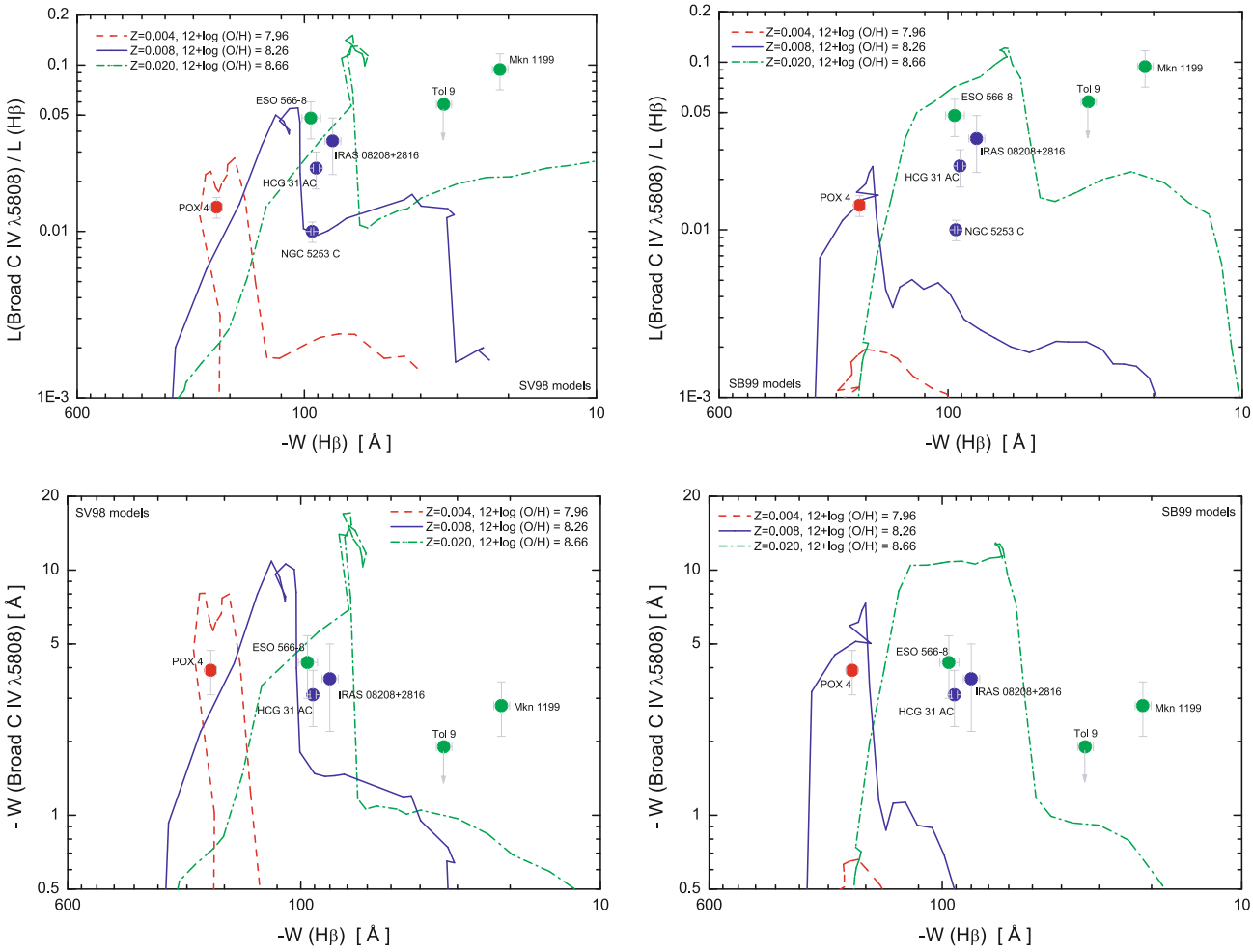

Fig. 8. Comparison of the observed intensities (*upper row*) and equivalent width (*lower row*) of the broad He II λ4686 emission line with the predictions given by SV98 (*left*) and SB99 (*right*) models. Symbols are the same as in Fig. 6.

nebular He II line at high metallicities, as Guseva et al. (2000) previously noticed. These authors also pointed out that objects with detected and nondetected WR features mingle indistinctly in these plots, and hence not only WR stars but also O stars may be contributing to the ionization of the He^+. Precisely this was one of the conclusions reached by BKD08, as we already discussed in Sect. 4.

Figure 7 compares the observed intensities and equivalent width of the broad He II λ4686 emission line with the predictions given by SV98 and SB99 models. Again the theoretical predictions agree well with the observational data, but we observe that the solar-metallicities model clearly overpredict the broad He II λ4686 intensities and equivalent widths by a factor 4–8. Although part of this disagreement maybe a consequence of the more complex star-formation histories of the high-metallicity galaxies (and hence an increase of the W(Hβ) because of the higher importance of older stellar populations), we consider that some of the disagreement between predictions and observational data is real. Pindao et al. (2002) also reported that theoretical models overestimate the WR fluxes in solar and super-solar metallicity objects.

Actually, we hold that the agreement we see at low metallicities may be just incidental. The SV98 and SB99 models consider the solar values of the intensities of the broad WR lines independently of the metallicity, but as we explained before (Sect. 5) they are drastically reduced at low metallicities. Therefore, the predictions given by these models *should not* agree with the observational data at low metallicities. Hence, models using the same parameters as SV98 and SB99 do agree but including metallicity-dependent WR line luminosities would *underpredict* the observed broad He II λ4686 intensity (and its equivalent width). For example, considering the formulae presented before (Eq. (7)), the model with 12 + log(O/H) = 7.96 (red dashed line in the figures) would predict broad He II intensities that are 65% of the intensities shown in Fig. 7, which makes their equivalent widths also much lower than those seen in the figure.

The same situation is found when comparing the observed broad C IV λ5808 emission line with the model predictions (Fig. 8). For example, for the central burst in POX 4, the predicted I(C IV λ5808)/I(Hβ) is ~0.015 following the SV98 models, quite in agreement with the actual value observed in this object (0.014). Considering the effect of lower WR luminosities at lower metallicities (Eq. (8)), the value predicted by the models should be ~0.01, which is around 70% of the observed value. Hence, the SV98 and SB99 theoretical models are indeed underpredicting the intensities of the broad WR lines at low metallicities. This result agrees with that reported by BKD08 and previously noticed by other authors (e.g. Legrand et al. 1997; Guseva et al. 2000). The best explanation of this discrepancy seems to be that the binary channel for producing WR stars is important

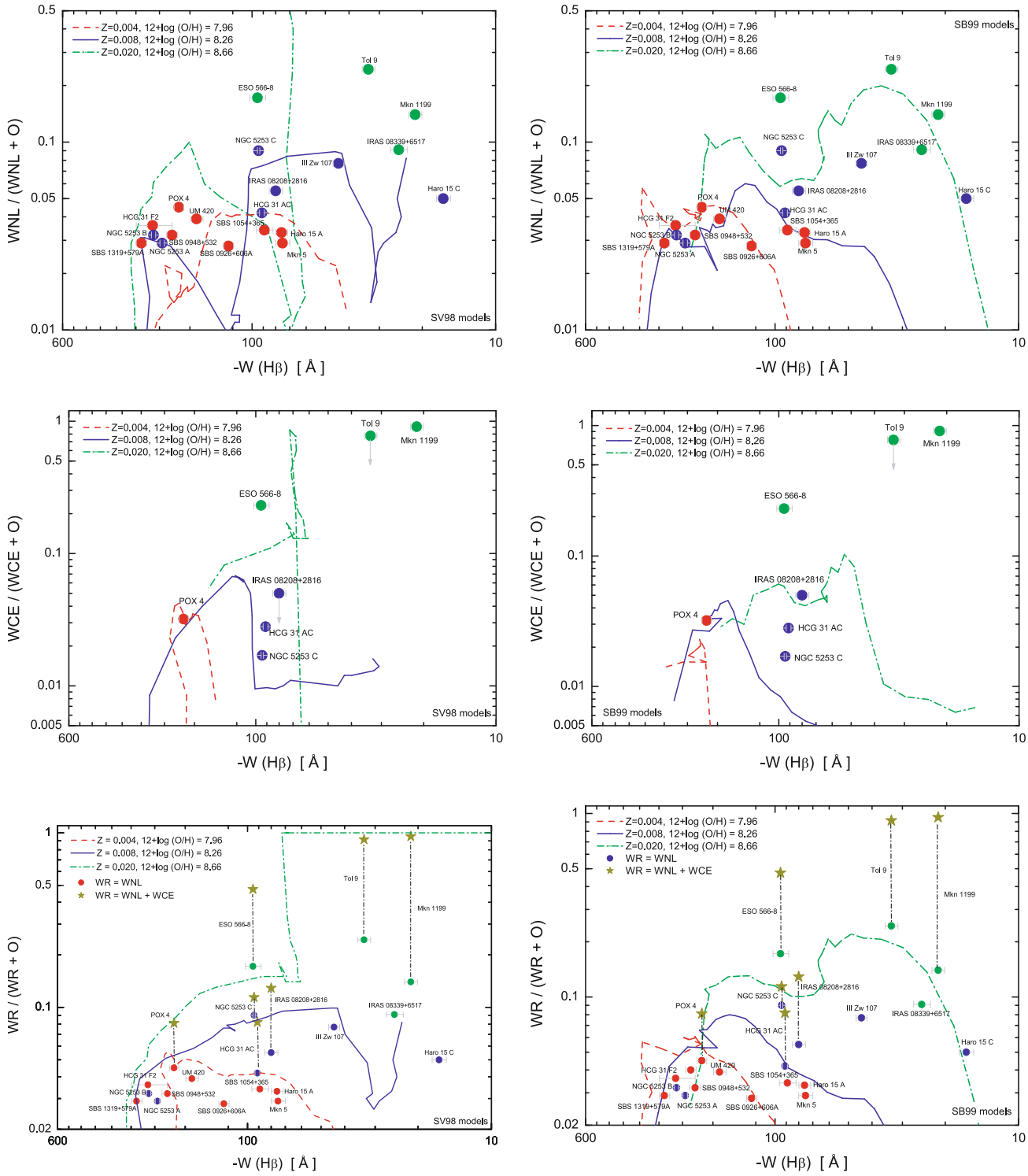

Fig. 9. Comparison of the WNL/(WNL+O) (*upper row*) WCE/(WCE+O) (*central row*) and WR/(WR+O) (*lower row*) ratios with the predictions given by SV98 (*left*) and SB99 (*right*) models. Symbols are the same as in Fig. 6.

at low metallicities, so that single star models are not efficient enough to reproduce the observed values. The inclusion of binaries in the models led to a prolongated WR phase (van Bever & Vanbeveren 2003) and to an increase in the WR/(WR+O) ratio (Eldridge et al. 2008). The binary channel ingredient should be taken into account in new models of evolving starbursts showing WR features, as it has not been included before, although there is some work in process (Eldridge & Stanway 2009). These new models should also consider the metallicity dependence of the WR luminosities.

Besides this problem, from Fig. 8 is also clear that the predictions given by the SB99 models are worse than those predicted by the SV98 models. The SB99 predictions quite disagree for low- and intermediate-metallicity objects. Even without considering the diminution of the WR luminosities, the SB99 models predict I(C IV λ5808)/I(Hβ) ~ 0.2 for POX 4, which is only the

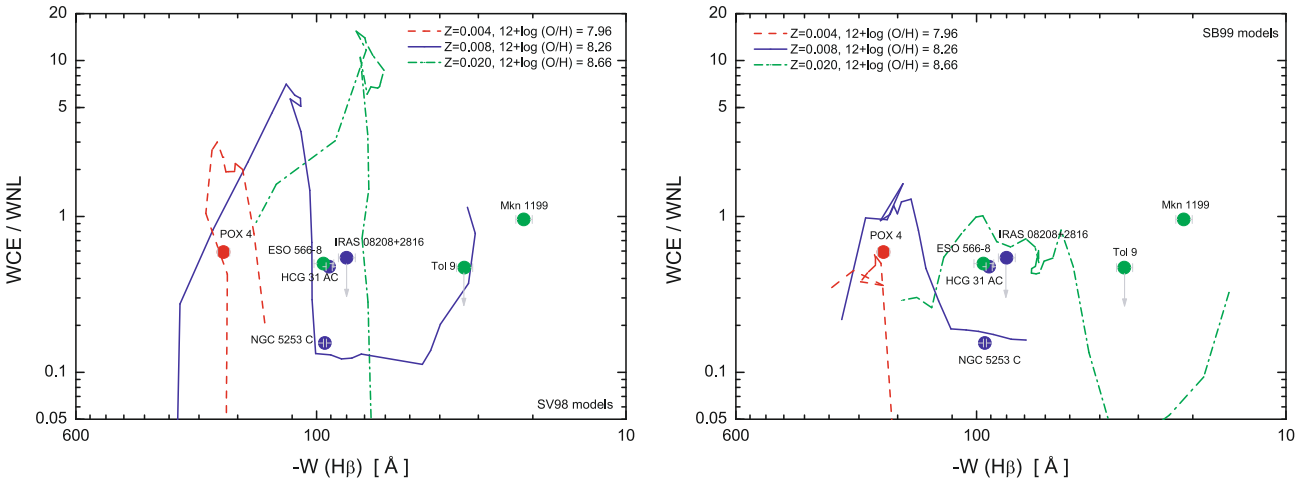

Fig. 10. Comparison of the derived WCE/WNL ratios with the predictions given by the SV98 (*left*) and SB99 (*right*) models. Symbols are the same as in Fig. 6.

14% of the observed value. Hence we suggest that we detect more WCE stars than those predicted by the models, which difference is even more pronounced at lower metallicities.

Let us now compare the observed WR/(WR+O) ratios with the theoretical predictions (Fig. 9). The numbers of WNL and WCE stars predicted by the models do not depend on the luminosities of the broad emission features assumed for a single WR star (only the predicted WR luminosities depend on them) and hence the comparison with our observational data should be still valid. The SB99 models better reproduce the WNL/(WNL+O) ratio than the SV98 models (Fig. 9, top row): the WNL/(WNL+O) ratio predicted by the SB99 models agrees well with the observed values for all metallicities, while the SV98 models underestimate the $W(\mathrm{H}\beta)$ in which the maximum of the WR/(WR+O) ratio is expected, which is very evident at low metallicities (differences >100 Å). If our observational points were affected by underlying absorption, this effect would be even higher. However, both kinds of models strongly disagree with the observations at high metallicities when compared with the observed WCE/(WCE+O) ratio (Fig. 9, central row). The disagreement is particularly important (more than one order of magnitude) for Mkn 1199.

The lower row in Fig. 9 shows the comparison of the derived WR/(WR+O) ratio with the theoretical predictions given by SV98 and SB99. In both cases we considered the ratios involving WNL and WR = WNL + WCE stars. The number of WCE stars estimated for Tol 9 and IRAS 08208+2816 is tentative, so their derived WR/(WR+O) ratio is an upper limit to the real one. As we commented before, there is a disagreement between the SV98 predictions and the observations at low metallicities, as these tend to show higher $W(\mathrm{H}\beta)$ values for the derived WR/(WR+O) ratio. If WCE are typically present in those bursts, the models would also underpredict the WR/(WR+O) ratio. Considering again the low-metallicity galaxy POX 4, the SV98 predictions for its WR/(WR+O) ratio are ~4 times smaller than the observed value considering the detection of both WNL and WCE stars in this object. This difference is also observed in objects with intermediate metallicites, although SV98 models work better in the solar-metallicity range.

On the other hand, the SB99 models seem to overpredict the WR/(WR+O) ratio at low luminosities. As we saw that the observed WNL/(WNL+O) ratio agrees well with the predictions in SB99 models, we may interpret this result in two ways: (i) models are overpredicting the number of WCE stars or (ii) we are not detecting WCE stars in these low-metallicity objects. In the only low-metallicity galaxy where we detect both WNL and WCE stars the agreement is not bad: the SB99 models account for around 80% of the WR population detected in POX 4. As we see, in all regions in which both subtypes of WR stars are detected the models underestimate the total number of WR stars. Hence the problem seems to be a consequence of the predictions of the number of WCE stars, but no the number of WNL stars. As we will see below, the derived WNL/WCE ratio computed for these objects is higher than that predicted by more recent models (Meynet & Maeder 2005; Eldridge & Vink 2006) and also higher than that empirically found counting individual WR stars in nearby galaxies.

8. The WCE/WNL ratio

Table 2 compiles the WCE/WNL ratio computed in the galaxies for which both WNL and WCE stars have been detected. Figure 10 compares the WCE/WNL ratios with the results given by the SV98 and SB99 models. The SV98 models clearly predict an increase of the maximum of the WCE/WNL ratio with increasing metallicity, but that is not seen in the SB99 models. Actually, the predictions given by these two kinds of models clearly disagree. The SV98 models seem to better reproduce the observed ratios at low and intermediate metallicities, but because of all the caveats about the predictions of the numbers of WNL and WCE stars we consider that the SV98 and SB99 models are not valid.

A much more interesting analysis is the metallicity-dependence of the WCE/WNL ratio. Figure 11 shows the WCE/WNL ratio as a function of the oxygen abundance for our starbursting galaxies (blue circles) and its comparison with the values obtained for nearby spiral (red squares) and irregular (yellow stars) galaxies for which the WR content has been studied in detail (Crowther 2007). Except for the particular case of the starbursting Local Group galaxy IC 10 (Massey & Holmes 2002; Crowther et al. 2003), for which the true WR populations are still somewhat uncertain, the WCE/WNL ratio clearly increases with the metallicity. That trend also agrees with the SV98 and SB99 models predictions (not shown in Fig. 11), for example,

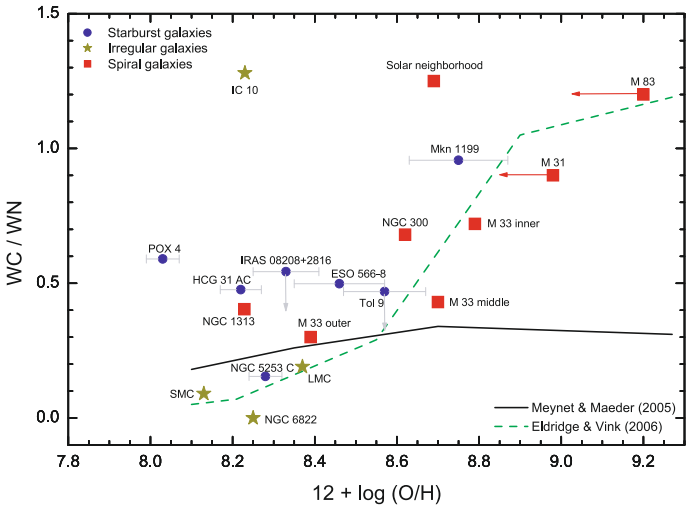

Fig. 11. Comparison between the observed WCE/WNL ratio and the metallicity for the starburst galaxies analyzed in this work (blue circles). We include the WC/WN ratios derived for nearby spiral (red squares) and irregular (yellow stars) galaxies (Massey & Johnson 1998; Crowther et al. 2003, 2007; Schild et al. 2003; Hadfield et al. 2005; Hadfield & Crowther 2007). Several regions within M 33 are shown because of the strong metallicity gradient in this galaxy. The evolutionary model predictions by Meynet & Maeder (2005, black continuous line) including rotation and Eldridge & Vink (2006, green dashed line) including a metallicity-dependence of the WR winds are also shown.

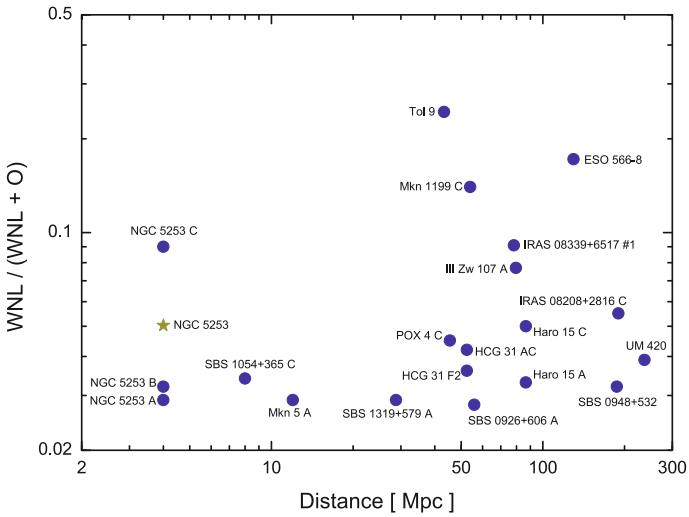

Fig. 12. WNL/(WNL+O) ratio vs. the distance to the galaxies. Notice that we also indicate the region within the galaxy in which the WR features are detected. The average value of the WNL/(WNL+O) ratio for the BCDG NGC 5253 is plotted with a yellow star.

the maximum of the WR/(WR+O) ratio in SV98 models increases from 0.025 to 1 between metallicities of 7.36 and 8.96 – in units of 12 + log(O/H)–, respectively. Following Crowther (2007), we plot in Fig. 11 the predictions given by the most recent WR models, Meynet & Maeder (2005), which allow for rotational mixing but without a WR metallicity dependence, and Eldridge & Vink (2006), which neglect rotational mixing but include a metallicity-scaling for WR stars. At high metallicities, the Eldridge & Vink (2006) models agree well with previous observations and also with our value for Mkn 1199, a spiral galaxy experiencing a strong star-formation event because of the interaction with a nearby companion (see Papers I and II).

However, the situation is quite different in the intermediate- and low-metallicity regime. Previous data of spiral and irregular galaxies agree well with both kind of models, but except for region C within NGC 5253, they clearly underestimate the WCE/WNL ratio in our sample of starburst galaxies. That is the same result that Guseva et al. (2000) found in their analysis. They assumed that the WC/WN ratio empirically derived by counting individual WR stars in nearby galaxies corresponds to continuous star formation, that should be ∼0 for galaxies with 12 + log(O/H) < 8.1. But low-metallicity galaxies are experiencing an instantaneous starburst, and hence their derived WCE/WNL may be as high as ∼3 for $Z = 0.004$ – 12 + log(O/H) ∼ 7.96 – according to SV98 models. This observation also agrees very well with the high ratio derived for IC 10, WCE/WNL ∼ 1.25. We therefore conclude that the differences in the WCE/WNL ratio found between starbursting low-metallicity dwarf galaxies and the typical nearby star-forming galaxies are a consequence of their very different star-formation histories, and that new models should definitively include this component.

However, we must keep in mind the effect of the slit position and the size of the aperture on the derived WR properties, which is particularly evident in nearby objects such as IC 10 or NGC 5253. Indeed, we see that different regions within these galaxies have very different WR populations. To investigate this issue, we plot in Fig. 12 the metallicity-dependence WNL/(WNL+O) ratio as a function of the distance to the galaxies (see Table 1 in Paper I). The distance range of our sample galaxy is between 4 Mpc (NGC 5253) and 237 Mpc (UM 420), with the majority of the objects within a distance of 100 Mpc. We do not see any clear correlation in this diagram, so we can discard any distance effect in our conclusions. We remind that we did not consider all flux of the galaxy with a fixed aperture, but analyzed the spectra of the brightest H II regions found in each galaxy using our Hα maps (Paper I) and choosing the size of the aperture according to these regions (Paper II). Hence the effects of dilution of the WR features (including areas in which the WR stars are not presented) were minimized in our analysis.

9. The WR dependence on the IMF

The detection of WR stars of both WN and WC subtypes and the derived WC/WN ratio provides strong constraints for stellar evolution models through the determination of the upper cut-off limit of the IMF. As WC stars are difficult to observe in low-metallicity environments, these studies are usually performed in metal-rich objects. Actually, the slope of the IMF and its dependence on metallicity is still a controversial issue. Some studies support a Salpeter-like IMF at solar metallicities (Bresolin & Kennicutt 2002; Pindao et al. 2002; Fernandes et al. 2004; Bresolin et al. 2005), but other observations have questioned this assumption at different metallicities. Schaerer et al. (1999) and Huang et al. (1999) suggested a flatter IMF at lower metallicities. Fernandes et al. (2004) underlined a dependence of the IMF slope on galaxy metallicity, in which low metallicity galaxies show a Salpeter-like IMF while high-metallicities galaxies either show a steeper IMF or experience an extended burst. A somewhat similar result was recently found by Zhang et al. (2007), who found that the IMF slope increases with increasing metallicity, with the slope index ranging from $\alpha \sim 1.0$ for $Z = 0.001$ to $\alpha \sim 3.3$ for $Z = 0.020$.

BKD08 pointed out that taking into account the considerable number of parameters that should be considered when modeling starbursts with significant WR populations (age of the burst,

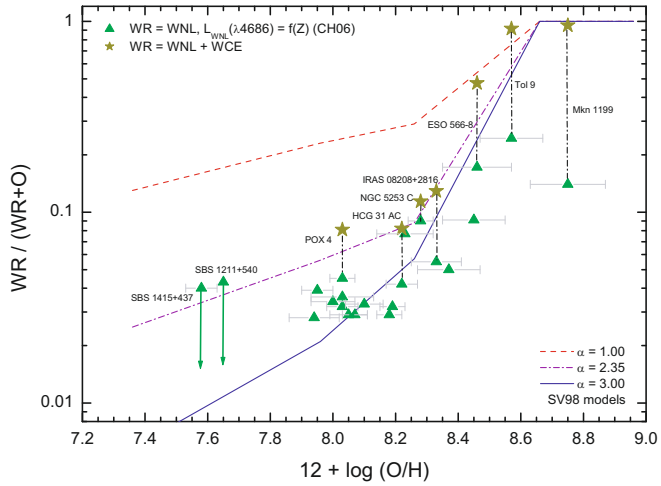

Fig. 13. WR/(WR+O) vs. metallicity and the predictions of SV98 models assuming three different IMFs, $\alpha = 1.00$ (flatter, red dashed line), 2.35 (Salpeter, dashed-dotted purple line) and 3.00 (steeper, blue continuous line). As in Fig. 5, green triangles indicate WR = WNL considering a metallicity-dependent broad He II λ4686, and dark yellow stars plot WR = WNL + WCE assuming the metallicity-dependence of both WNL and WCE luminosities. Dashed lines connect the WR = WNL and the WR = WNL + WCE values for the galaxies for which we have WCE data, these objects have been labelled. We include the upper limit to the WR/(WR+O) ratio estimated for the very low-metallicity galaxies SBS 1211+540 and SBS 1415+437.

star-formation history, metallicity, dependence of the WR features on stellar rotation and wind loss, inclusion of the binary channel...) it is not a good idea to include the slope of the IMF as an additional parameter. Just as an exercise, we compared the predictions given by SV98 models for an instantaneous burst with the same properties we explained before but changing the slope of the IMF, $\alpha = 1.00$, 2.35 (Salpeter) and 3.00. Figure 13 plots the observed WR/(WR+O) ratio versus the oxygen abundance and the maximum of the WR/(WR+O) predicted by these three models. The observational data plotted in this figure are the same as in Fig. 5; the WNL and WCE stars numbers were computed assuming a metallicity-dependent luminosity of the WR features, as we explained before. As we see, models with flatter IMFs tend to predict higher WR values and at all metallicities, so that a flat IMF implies a relatively large population of massive stars, leading to a larger WR population.

From Fig. 13 is evident that our data do not support the hypothesis that low-metallicity objects have flatter IMFs. Actually it is quite the opposite, the model with $\alpha = 3.00$ seems to agree better with the data. The assumption of metallicity-independent WR luminosities would move our data points to lower WR/(WR+O) values, and hence favore an even steeper slope for the IMF at low metallicities. However, we notice that the majority of the data points assumes WR = WNL, but we have seen that the WCE stars should have a non-negligible contribution to the total WR star population even at low metallicities. Actually, the model with a Salpeter-like IMF agrees very well with the observed WR/(WR+O) value of the objects for which we have detected both WNL and WCE stars. We then conclude that the assumption of a Salpeter-like IMF is valid and that the metallicity-dependence on the WR luminosities is probably playing a key factor in the discrepancies between data and models found by Zhang et al. (2007).

A final remark about IMFs in star-forming galaxies. Recent studies (Weidner & Kroupa 2005, 2006) have revealed that the total stellar population of the new formed stars of all young star clusters within the same galaxy follows a distribution function steeper than the canonical IMF in the high-mass regime. The so-called *integrated galactic initial mass function* (IGIMF) deviates increasingly from the underlying canonical IMF with decreasing star-formation and total galaxy mass. Blue Compact Dwarf galaxies, such as the typical low-metallicity objects in which WR stars are detected, should have a very different IGIMF than spiral galaxies like the Milky Way. This parameter should be therefore also considered when modelling the evolution of the stellar populations in starbursts and star-forming galaxies.

10. Conclusions

We presented a detailed analysis of the broad stellar features originated by winds of Wolf-Rayet stars in a sample of star-bursting galaxies previously classified as WR galaxies. The photometric properties of these galaxies were compiled in Paper I, while their spectroscopic analysis was shown in Paper II. The metallicity of these galaxies lies between 7.58 and 8.75 – in units of 12 + log(O/H)–. Our goals are to locate the WR-rich stellar clusters, derive the number of O, WN and WC stars and compare the results with previous observations and the predictions of evolutionary synthesis models. Our main results are the following:

1. The blue WR bump, mainly composed by the broad, stellar He II λ4686 emission line and attributed to WN stars, is unambiguously detected in 12 regions and it is probably observed in eight other regions. Aperture effects and/or the position of the slit within the starburst are clearly playing a fundamental role in the detection of the WR features. We consider that multi-aperture spectroscopy or narrow-band imagery using filters sensitive to WR features and the adjacent continuum later followed by slit spectroscopy may be more appropriate for this kind of analysis. The advent of the optical 3D spectroscopy is already showing the localization of WR features with star-forming regions (i.e. Kehrig et al. 2008; García-Lorenzo et al. 2008; James et al. 2009, 2010; López-Sánchez et al. 2010).
2. The broad C IV λ5808 emission line (red WR bump), attributed to WC stars, is clearly detected in four regions, and it is probably observed in two other objects.
3. We have performed a detailed fitting of the spectra considering the broad stellar and narrow nebular emission lines in both the blue and the red WR bumps. In the blue WR bump we usually found a contribution of the nebular and broad He II λ4686 components.
4. The nebular He II λ4686 is detected in 17 regions and it is probably observed in six other knots. We confirm the trend that galaxies with lower metallicities have a higher I(nebular He II λ4686)/I(Hβ) ratio. Some of our lowest-metallicity regions show the nebular but not the broad He II emission line. The SV98 models seem to underpredict the intensity of this emission line in low metallicity objects. Both findings agree with the conclusions reached by BKD08, who suggested that O stars and not only WR stars contribute to the ionization of the He^+ at low metallicities.
5. We used the intensity ratios of the broad He II λ4686 and C IV λ5808 lines to derive the number of O, WN and WC stars within each region. We have considered two methods: (i) assuming constant luminosities for the WR features,

as it is commonly done and it used in theoretical models, and (ii) assuming metallicity-dependent luminosities for the WR features, as both recent observations and new WR stars models indicate (CH06). This second method gives higher number of WR stars at lower metallicities. We derive an empirical estimation of the WNL/(WNL+O) ratio using the intensity of the broad He II λ4686 line assuming the metallicity-dependent of the WR luminosities.

6. As expected following theoretical models, the total number of WR stars increases with increasing metallicity. However, we observe a possible flattening of the WR/(WR+O) ratio for objects with $12+\log(O/H) < 8.2$, because all the low-metallicity galaxies show a constant value of ~0.03–0.04, but more data are needed to confirm this trend. We also conclude that the contribution of the WCE stars is not negligible at low metallicities.
7. The comparison of the observational data with the theoretical predictions given by the most accurate models available to date, SV98 and SB99, is difficult because of all the parameters involved, namely, age, metallicity, star-formation history, assumption of the IMF and WR stars properties (variation of the WR luminosities with the metallicity, effect of star rotation, contribution of the WR binnary channel). New models including all these factors are absolutely needed to perform an appropriate comparison with the observational data. The available SV98 and SB99 models seem to work better at higher metallicities, but more complex star-formation histories are needed to explain the observed WR luminosities and ratios in this regime. At low metallicities the SV98 and SB99 models fail to reproduce the observed WR intensities because these models do not consider the decreasing of the WR luminosities with decreasing metallicity. Our data agree with the SV98 models considering a Salpeter-like IMF for all metallicites.
8. Finally, the WCE/WNL ratios observed in our starbursting galaxies are quite different than those empirically found in nearby star-forming and irregular galaxies. We consider that this effect is a consequence of the very different star-formation histories that these objects are experiencing.

Acknowledgements. We are very grateful to the referee, Daniel Kunth, who helped us to improve the quality of this manuscript. Á.R.L.-S. *deeply* thanks to Universidad de La Laguna (Tenerife, Spain) for forcing him to translate his Ph.D. Thesis from English to Spanish; he had to translate it from Spanish to English to complete this publication. Á.R.L-S. also thanks to all the people at the CSIRO/Australia Telescope National Facility, especially to Bärbel Koribalski, for their support and friendship while translating his Ph.D. The authors are very grateful to A&A language editor, A. Peter, for her kind revision of the manuscript. This work has been partially funded by the Spanish Ministerio de Ciencia y Tecnología (MCyT) under project AYA2004-07466. This research has made use of the NASA/IPAC Extragalactic Database (NED) which is operated by the Jet Propulsion Laboratory, California Institute of Technology, under contract with the National Aeronautics and Space Administration. This research has made extensive use of the SAO/NASA Astrophysics Data System Bibliographic Services (ADS).

References

Abbott, D. C. 1982, ApJ, 263, 723
Allen, D. A., Wright, A. E., & Goss W. M. 1976, MNRAS, 177, 91
Arnault, Ph., Kunth, D., & Schild, H. 1989, A&A, 224, 73
Asplund, M., Grevesse, N., & Sauval, A. J. 2005, in Cosmic Abundances as Records of Stellar Evolution and Nucleosynthesis, ed. F. N. Bash, & T. G. Barnes (San Francisco: ASP), ASP Conf. Ser., 335, 25
Bresolin, F., & Kennicutt, R. C. Jr. 2002, ApJ, 572, 838
Bresolin, F., Kennicutt, R. C. Jr., & Garnett, D. R. 1999, ApJ, 510, 104
Bresolin, F., Schaerer, D., González -Delgado, R. M., & Stasińska, G. 2005, A&A, 441, 981
Brinchmann, J., Kunth, D., & Durret, F. 2008, A&A, 485, 657 (BKD08)
Brown, T. M., Heap, S. R., Hubeny, I., Lanz, T., & Lindler, D. 2002, ApJ, 579, 75
Bruzual, G., & Charlot, S. 2003, MNRAS, 344, 1000 (BC03)
Buckalew, B. A., Kobulnicky, H. A., & Dufour, R. J. 2005, ApJS, 157, 30
Cairós, L. M., Caon, N., Vílchez, J. M., González-Pérez, J. N., & Muñoz-Tuñón, C. 2001, ApJS, 136, 393
Cairós, L. M., Caon, N., García-Lorenzo, B., et al. 2007, ApJ, 669, 251
Cerviño, M., & Mas-Hesse, J. M. 1994, A&A, 284, 749
Cerviño, M., Mas-Hesse, J. M., & Kunth, D. 2002, A&A, 392, 19
Contini, T. 1996, Liege International Astrophysical Colloquia 33: Wolf-Rayet stars in the framework of stellar evolution, Liege: Université de Liege, Institut d'Astrophysique, ed. J. M. Vreux, A. Detal, D. Fraipont-Caro, E. Gosset, & G. Rauw, 619
Conti, P. S., 1976, MSRSL, 9, 193
Crowther, P. A. 2007, ARA&A, 45, 177
Crowther, P. A., & Bibby, J. L. 2009, A&A, 499, 455
Crowther, P. A., & Hadfield, L. J., 2006, A&A, 449, 711 (CH06)
Crowther, P. A., Drissen, L., Abbott, J. B., Royer, P., & Smartt, S. J. 2003, A&A, 404, 483
Crowther, P. A., Carpano, S., Hadfield, L. J., & Pollock, A. M. 2007, A&A, 469, L31
De Mello, D. M., Schaerer, D., Heldmann, J., & Leitherer, C. 1998, ApJ, 507, 199
Dinerstein, H. L., & Shields G. A. 1986, ApJ, 311, 45
Eldridge, J. J., & Stanway, E. R. 2009, MNRAS, 400, 1019
Eldridge, J. J., & Vink, J. S. 2006, A&A, 452, 295
Eldridge, J. J., Izzard, R. G., & Tout, C. A. 2008, MNRAS, 384, 1109
Fernandes, I. F., de Carvalho, R., Contini, T., & Gal, R. R. 2004, MNRAS, 355, 728
Fioc, M., & Rocca-Volmerange, B. 1997, A&A, 326, 950
García-Vargas, M., Bressan, A., & Díaz, A. I. 1995, A&AS, 112, 13
García-Lorenzo, B., Cairós, L. M., Caon, N., Monreal-Ibero, A., & Kehrig, C. 2008, ApJ, 677, 201
Garnett, D. R. 2003, lectures on Cosmochemistry: The melting pot of the elements, XIII Canary Islands Winter School of Astrophysics, Puerto de la Cruz, Tenerife, Spain, November 19–30, 2001, ed. C. Esteban, R. J. García López, A. Herrero, & F. Sánchez, Cambridge Contemporary Astrophysics (Cambridge, UK: Cambridge University Press), 171
Garnett, D. R., Kennicutt, R. C. Jr., Chu, Y.-H., & Skillman E. D. 1991, ApJ, 373, 458
Gil de Paz, A., & Madore, B. F. 2005, ApJS, 156, 345
Guseva, N., Izotov, Y. I., & Thuan, T. X. 2000, ApJ, 531, 776
Guseva, N. G., Izotov, Y. I., Papaderos, P., et al. 2001, A&A, 378, 756
Hadfield, L. J., & Crowther, P. A. 2006, MNRAS, 368, 1822
Hadfield, L. J., & Crowther, P. A. 2007, MNRAS, 381, 418
Hadfield, L. J., Crowther, P. A., Schild, H., & Schmutz, W. 2005, A&A, 439, 265
Hjorth J., et al. 2003, Nature, 423, 847
Huang, J. H., Gu, Q. S., Ji, L., et al. 1999, ApJ, 513, 215
Izotov, Y. I., & Thuan, T. X. 1999, ApJ, 511, 639
Izotov, Y. I., Foltz, C. B., Green, R. F., Guseva, N. G., & Thuan T. X., 1997, ApJ, 487, L37
Izotov, Y. I., Chaffee, F. H., Foltz, C. B., et al. 1999, ApJ, 527, 757
James, B. L., Tsamis, Y. G., Barlow, M. J., et al. 2009, MNRAS, 398, 2
James, B. L., Tsamis, Y. G., & Barlow, M. J. 2010, MNRAS, 401, 759
Kehrig, C., Vílchez, J. M., Sánchez, S. F., et al. 2008, A&A, 477, 813
Kong, X., Cheng, F. Z., Weiss, A., & Charlot, S. 2002, A&A, 396, 503
Krüger, H., Fritze-v. Alvensleben, U., Frike, K. J., & Loose, H. H. 1992, A&A, 259, L73
Kunth, D., & Joubert, M. 1985, A&A, 142, 411
Kunth, D., & Sargent, W. L. W. 1981, A&A, 101, 5
Kunth, D., & Schild, H. 1986, A&A, 169, 71
Legrand, F., Kunth, D., Roy, J.-R., Mas-Hesse, J. M., & Walsh, J. R. 1997, A&A, 326, 17
Leitherer, C., & Heckman, T. M. 1995, ApJS, 96, 9
Leitherer, C., Schaerer, D., Goldader, J. D., et al. 1999, ApJS, 123, 3 (STARBURST 99)
López-Sánchez, Á. R. 2006, Ph.D. Thesis, Universidad de la Laguna, Tenerife, Spain
López-Sánchez, Á. R. 2010, A&A, accepted (Paper V)
López-Sánchez, Á. R., & Esteban, C. 2008, A&A, 491, 131 (Paper I)
López-Sánchez, Á. R., & Esteban, C. 2009, A&A, 508, 615 (Paper II)
López-Sánchez, Á. R., & Esteban, C. 2010, A&A, accepted (Paper IV)
López-Sánchez, Á. R., Esteban, C., & Rodríguez, M. 2004a, ApJS, 153, 243
López-Sánchez, Á. R., Esteban, C., & Rodríguez, M. 2004b, A&A, 428, 445
López-Sánchez, Á. R., Esteban, C., & García-Rojas, J. 2006, A&A, 449, 997
López-Sánchez, Á. R., Esteban, C., García-Rojas, J., Peimbert, M., & Rodríguez, M. 2007, ApJ, 656, 168

López-Sánchez, Á. R., Mesa-Delgado, A., López-Martín, L., & Esteban, C. 2010, in preparation
Maeder, A. 1981, A&A, 102, 401
Maeder, A. 1990, A&AS, 84, 139
Maeder, A. 1991, A&A, 242, 93
Maeder, A., & Meynet, G. 2005, A&A, 440, 1041
Massey, P., & Johnson, O. 1998, ApJ, 505, 793
Massey, P., & Holmes, S. 2002, ApJ, 580, 35
Mas-Hesse, J. M., & Kunth, D. 1991, A&AS, 88, 399
Mas-Hesse, J. M., & Kunth, D. 1999, A&A, 349, 765
Meynet, G. 1995, A&A, 298, 767
Meynet, G., & Maeder, A. 2005, A&A, 429, 581
Pakull, M. W., & Angebault, L. P. 1986, Nature, 322, 511
Papaderos, P., Izotov, Y. I., Guseva, N. G., Thuan, T. X., & Fricke, K. J. 2006, A&A, 454, 119
Pérez-Montero, E., & Díaz, A. I. 2007, MNRAS, 377, 1195
Pindao, M., Schaerer, D., González-Delgado, R. M., & Stasińska, G. 2002, A&A, 394, 443
Schaerer, D. 1996, ApJ, 467, 17
Schaerer, D. 1998, HiA, 11, 134
Schaerer, D., & Vacca, W. D. 1998, ApJ, 497, 618 (SV98)
Schaerer, D., de Koter, A., Schmutz, W., & Maeder, A. 1996, A&A, 312, 475
Schaerer, D., Contini, T., Kunth, D., & Meynet, G. 1997, ApJ, 481, L75
Schaerer, D., Contini, T., & Pindao, M. 1999, A&AS, 136, 35
Schaerer, D., Guseva, N. G., Izotov, Yu. I., & Thuan, T. X. 2000, A&A 362, 53
Schild, H., Crowther, P. A., Abbott, J. B., & Schmutz, W. 2003, A&A, 397, 859
Smith, L. J., Norris, R. P. F., & Crowther, P. A. 2002, MNRAS, 337, 1309
Stasiǹska, G. 1998, Abundance Profiles: Diagnostic Tools for Galaxy History, ASP Conf. Ser., 147, 142
Stasińska, G., & Izotov, Y., 2003 A&A, 397, 71
Stasińska, G., Schaerer, D., & Leitherer, C. 2001, A&A, 370, 1
Thuan, T. X., & Izotov, Y. I. 2005, ApJS, 161, 240
Vacca, W. D. 1994, ApJ, 421, 140
Vacca, W. D., & Conti, P. S. 1992, ApJ, 401, 543
Vaceli, M. S., Viegas, S. M., Gruenwald, R., & De Souza, R. E. 1997, AJ, 114, 1345
van Bever, J., & Vanbeveren, D. 2000, A&A, 358, 462
van Bever, J., & Vanbeveren, D. 2003, A&A, 400, 63
Vanbeveren, D., van Bever, J., & Belkus, H. 2007, ApJ, 662, L107
Vázquez, G. A., & Leitherer, C. 2005, ApJ, 621, 695
Vink, J. S., & de Koter, A. 2005, A&A, 442, 587
Weidner, C., & Kroupa, P. 2005, ApJ, 625, 754
Weidner, C., & Kroupa, P. 2006, MNRAS, 365, 1333
Woodward P. R. 1978, ARA&A, 16, 555
Woosley, S. E., & Heger, A. 2006, ApJ, 637, 914
Zhang, W., Kong, X., Li, C., Zhou, H.-Y., & Cheng, F.-Z. 2007, ApJ, 655, 851